PHONON DRAG THERMOPOWER IN CADMIUM, ZINC AND MAGNESIUM

Thesis for the Degree of Ph. D.

MICHIGAN STATE UNIVERSITY

VINCENT ALAN ROWE

1967

THESIS

This is to certify that the

thesis entitled

PHONON DRAG THERMOPOWER
in
CADMIUM, ZINC and MAGNESIUM
presented by

Vincent Alan Rowe

has been accepted towards fulfillment
of the requirements for

Ph.D. degree in Physics

R. H. Schwacke
Major professor

Date August 29, 1967

O-169

ABSTRACT

PHONON DRAG THERMOPOWER

IN

CADMIUM, ZINC AND MAGNESIUM

by

Vincent Alan Rowe

Anisotropic thermopowers and thermal conductivities of single crystals of the three Group II metals Cd, Zn, and Mg have been measured from 1.25°K to room temperature. An attempt has been made to correlate the phonon drag thermopower in these metals with the detailed topologies of their Fermi surfaces.

PHONON DRAG THERMOPOWER
IN
CADMIUM, ZINC AND MAGNESIUM

by

Vincent Alan Rowe

A THESIS

Submitted to
Michigan State University
in partial fulfillment of the requirements
for the degree of

DOCTOR OF PHILOSOPHY

Department of Physics and Astronomy

1967

Acknowledgments

The assistance and encouragement of Professor P. A. Schroeder throughout all phases of this investigation is gratefully acknowledged. I am indebted to Professor F. J. Blatt for many illuminating discussions.

The work was supported by the National Science Foundation.

TABLE OF CONTENTS

TABLE OF CONTENTS, Continued

List of Figures

List of Tables

Appendices

1. Introduction

In 1963 Jan and Pearson[1] published the results of their investigation of the thermopower of intermetallic AuSn. Finding considerable anisotropy in the data taken on crystals of differing orientations, they attempted to deduce a topology for the Fermi surface of AuSn consistent with their results.

We felt, however, with the present limited understanding of phonon drag thermopower that it would be more logical to work with metals with known Fermi surfaces and try to correlate detailed features of these surfaces with their observed phonon drag thermopowers. This project was therefore commenced with a view to testing the hypothesis that various sheets of the Fermi surface would make discernible contributions to the phonon drag thermopower. We established four criteria for the choice of metals on which to take these phonon drag thermopower measurements: (1) the Fermi surfaces should be well established, (2) more information would accrue if the materials studied were not cubic --thus resulting in an anisotropic thermopower, (3) oriented single crystals of fairly high purity are required if advantage of number (2) is to be taken and if the results are to clearly reflect the thermopower of the pure metals, (4) metals sufficiently alike are needed to facilitate comparison of the results.

The three group II metals, Cadmium, Zinc, and Magnesium

satisfy these criteria. Their Fermi surfaces are quite similar and well known. All have hexagonal symmetry and thus will have 2 independent thermoelectric coefficients. With the possible exception of Mg, all are fairly easy to obtain as oriented single crystals. Measurements on polycrystalline Cd wire had already been carried out in our laboratory. Figure 1-1 shows the interesting temperature dependence displayed by Cd in these results.

At the outset, we had hoped to be able to correlate the phonon drag thermopower with Fermi surface geometry, expecting the diffusion term to be a simple monotonically increasing function of temperature whose sign is determined at room temperature. As it turns out, one cannot be certain of the behavior of a diffusion thermopower arising from many sheeted Fermi surfaces such as those of the present metals.

Very few attempts to directly correlate transport properties with Fermi surface topology have been made to date. We mention work by Klemens[2] on the thermopower and resistivity of tin at low temperatures, Bailyn and Dugdale[3] on copper, and Ziman on noble metals[4].

We should point out that Gruneisen and Goens[5] measured the thermopowers of Cd and Zn from 20°K to room temperature in 1926. However, their data were taken with copper as the reference metal which has been shown to have an anomalous thermopower at low temperatures.

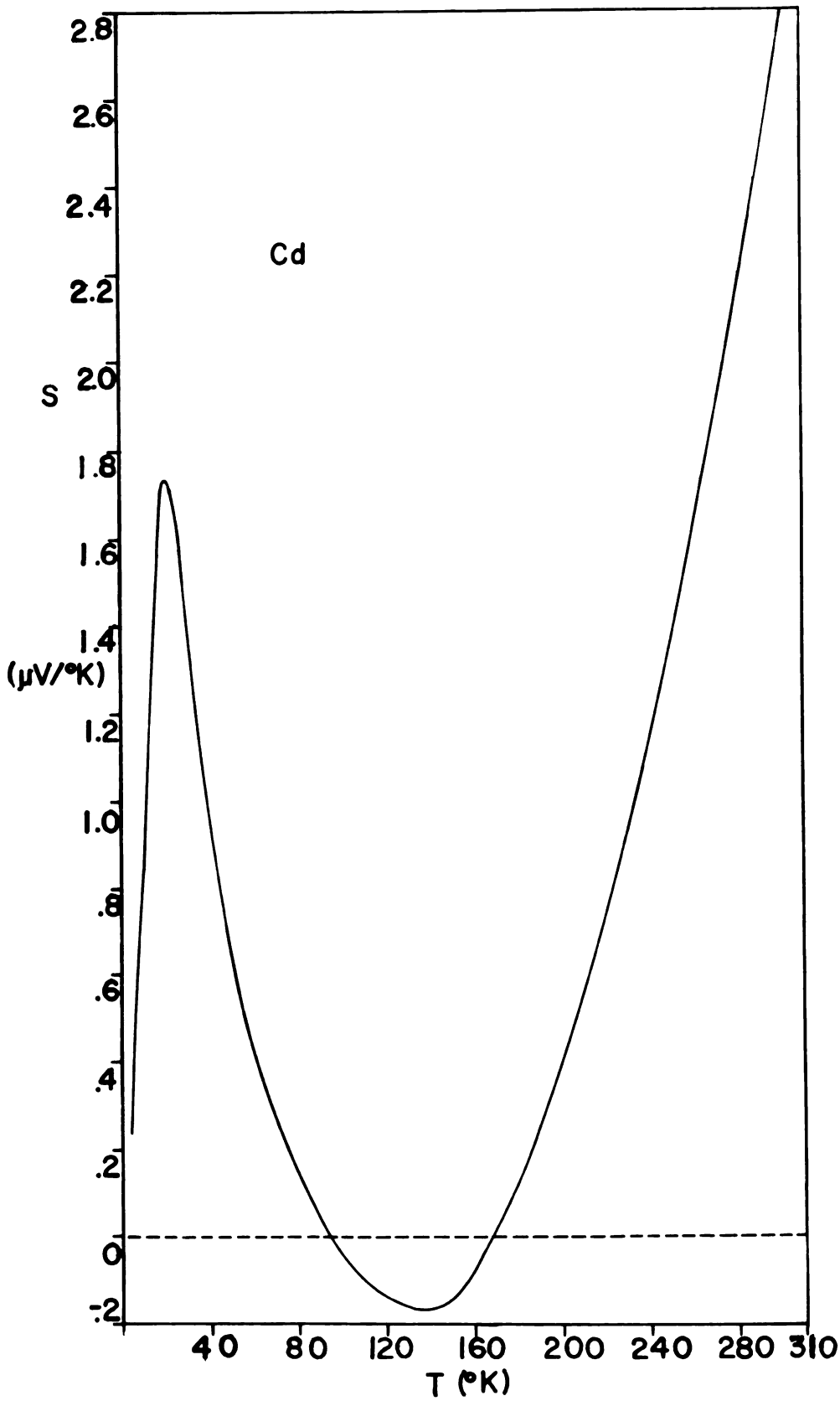
Cd
S
(μV/°K)
2.8
2.6
2.4
2.2
2.0
1.8
1.6
1.4
1.2
1.0
.8
.6
.4
.2
0
-.2
40
80
120
160
200
240
280
310
T (°K)

Fig. 1-1

We have also measured the thermal conductivity of each sample. For various reasons, however, this data was not found useful for the present purposes.

2. Theory

A. Thermoelectric Power - Thermodynamics

The theory of irreversible thermodynamics leads to the following equation:[6]

$$-\nabla\phi = -\frac{1}{e}\left[\underline{\underline{\Sigma}} \cdot \nabla T + \nabla\mu\right] \qquad 2\text{-I}$$

where ϕ is the scaler electric potential, e the electronic charge, $\underline{\underline{\Sigma}}$ the second rank thermoelectric tensor, T the absolute temperature and μ the chemical potential.

All the materials with which we are concerned being of hexagonal symmetry, the tensor takes the form:[7]

$$\underline{\underline{\Sigma}} = \begin{pmatrix} \Sigma_{\perp} & 0 & 0 \\ 0 & \Sigma_{\perp} & 0 \\ 0 & 0 & \Sigma_{\parallel} \end{pmatrix} \qquad 2\text{-II}$$

where $\parallel$ refers to the hexad axis, and $\perp$ refers to the basal plane. This implies that the various thermoelectric properties will be isotropic only in the basal plane.

Because of the basal plane isotropy, the problem may be reduced to 2 dimensions:

$$\begin{Bmatrix} \frac{\partial\phi}{\partial x} \\ \frac{\partial\phi}{\partial x} \end{Bmatrix} = \frac{1}{e}\left\{ \begin{pmatrix} \Sigma & 0 \\ 0 & \Sigma \end{pmatrix} \cdot \begin{Bmatrix} \frac{\partial T}{\partial x} \\ \frac{\partial T}{\partial x} \end{Bmatrix} + \begin{Bmatrix} \frac{\partial\mu}{\partial x} \\ \frac{\partial\mu}{\partial x} \end{Bmatrix} \right\} \qquad 2\text{-III}$$

Then, in the basal plane; for example:

$$\frac{\partial \phi}{\partial x} = \frac{1}{e} \Sigma_{\perp} \frac{\partial T}{\partial x} + \frac{1}{e} \frac{\partial u}{\partial x} \qquad 2\text{-IV}$$

To see the significance of equation 2-IV, consider the schematic circuit shown in Figure 2-1:

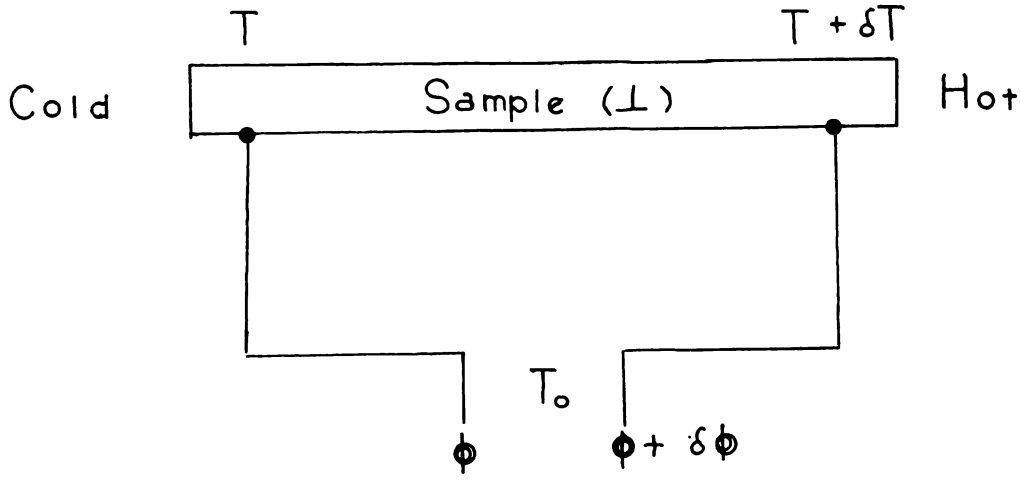

Figure 2-1

Suppose the sample axis coincides with some direction in the basal plane. Since lead is a cubic material its thermoelectric tensor is isotropic[8] with only one unique element, say Σ_{Pb}.

Let us integrate 2-IV around the circuit in Figure 2-1.

$$\int \frac{\partial \phi}{\partial x}\, dx = \frac{1}{e}\int \Sigma_{\perp}\frac{\partial T}{\partial x}\, dx + \frac{1}{e}\int \frac{\partial \mu}{\partial x}\, dx$$

or: 2-V

$$\int_{\phi}^{\phi+\delta\phi} d\phi = \int_{T_o}^{T} \Sigma_{Pb}dT + \int_{T}^{T+\delta T} \Sigma_{\perp}dT + \int_{T+\delta T}^{T_o} \Sigma_{Pb}\, dT + \int_{T_o}^{T_o} d\mu$$

The last term on the right vanishes because we have carried μ from T_o in lead to T_o in lead. The first and third terms on the right combine as follows:

$$\int_{T_o}^{T} \Sigma_{Pb}\, dT + \int_{T+\delta T}^{T_o} \Sigma_{Pb}\, dT = \cancel{\int_{T_o}^{T}} - \cancel{\int_{T_o}^{T}} - \int_{o}^{\delta T} = -\int_{o}^{\delta T} \Sigma_{Pb}\, dT$$

Similarly, the second term on the right:

$$\int_{T}^{T+\delta T} \Sigma_{\perp}\, dT = \int_{o}^{\delta T} \Sigma_{\perp}\, dT$$

Equation 2-V reduces, therefore, to:

$$\int_{\phi}^{\phi+\delta\phi} d\phi = \int_{o}^{\delta T} \frac{1}{e}(\Sigma_{\perp} - \Sigma_{Pb})\, dT$$

or for small δT

$$\delta\phi = \frac{1}{e}(\Sigma_{\perp} - \Sigma_{Pb})\ \delta T$$

or:

$$\frac{\delta\phi}{\delta T} = \frac{1}{e}(\Sigma_{\perp} - \Sigma_{Pb})$$

or setting $\frac{\Sigma_i}{e} = S_i$

$$S_{\perp} = \frac{\delta\phi}{\delta T} + S_{Pb} \qquad \text{2-VI}$$

Thus, $\Sigma_{\perp}$ is seen to be the usual absolute thermopower divided by the electric charge.

The case for $\Sigma_{||}$ follows along the lines of the above treatment.

Angular dependence of S:

These considerations do not allow for the case where the sample axis lies not along a symmetry direction but in some arbitrary direction relative to the principle axes. Figure 2-2 shows such an example.

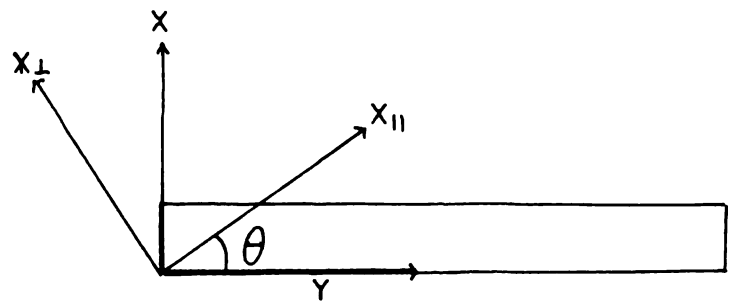

Figure 2-2

The coordinate transformation that expresses x, y in terms of $x_\perp$, $x_\parallel$ is:

$$\begin{Bmatrix} x \\ y \end{Bmatrix} = \begin{Bmatrix} \cos\theta & -\sin\theta \\ \sin\theta & \cos\theta \end{Bmatrix} \begin{Bmatrix} x_\perp \\ x_\parallel \end{Bmatrix}$$

Hence the thermoelectric tensor will have the following form in the (x,y) coordinate system:

$$\underline{\underline{\Sigma}}'(x,y) = \begin{Bmatrix} \cos\theta & -\sin\theta \\ \sin\theta & \cos\theta \end{Bmatrix} \begin{Bmatrix} \Sigma_\perp & 0 \\ 0 & \Sigma_\parallel \end{Bmatrix} \begin{Bmatrix} \cos\theta & \sin\theta \\ -\sin\theta & \cos\theta \end{Bmatrix}$$

$$= \begin{Bmatrix} \Sigma_\perp \cos^2\theta + \Sigma_\parallel \sin^2\theta & (\Sigma_\perp - \Sigma_\parallel)\cos\theta \sin\theta \\ (\Sigma_\perp - \Sigma_\parallel)\cos\theta \sin\theta & \Sigma_\perp \sin^2\theta + \Sigma_\parallel \cos^2\theta \end{Bmatrix}$$

In this instance 2-I becomes:

$$\begin{Bmatrix} \frac{\partial\phi}{\partial x} \\ \frac{\partial\phi}{\partial y} \end{Bmatrix} = \frac{1}{e}\,\Sigma'(x,y) \begin{Bmatrix} \frac{\partial T}{\partial x} \\ \frac{\partial T}{\partial y} \end{Bmatrix} + \frac{1}{e} \begin{Bmatrix} \frac{\partial\mu}{\partial x} \\ \frac{\partial\mu}{\partial y} \end{Bmatrix} \qquad \text{2-VII}$$

If we assume that with the heat current flowing along x, $\frac{\partial T}{\partial y} = o$ Then:

$$\frac{\partial\phi}{\partial x} = \frac{1}{e}\left\{\Sigma_\perp \cos^2\theta + \Sigma_\parallel \sin^2\theta\right\} \frac{\partial T}{\partial x} + \frac{1}{e}\frac{\partial\mu}{\partial x} \qquad \text{2-VIII}$$

From 2-VIII we then may deduce the thermoelectric power, bearing in mind the more specific results obtained in 2-VI.

$$S(\theta) = S_{\perp}\cos^2\theta + S_{\parallel}\sin^2\theta \qquad 2\text{-IX}$$

However, it is unrealistic to presume that in an anisotropic material thermal gradients will not persist in directions not parallel to the heat flow. Such gradients do in fact exist whenever the thermal conductivity is anisotropic. In our case the thermal conductivity tensor has the same form as the thermoelectric tensor and so is anisotropic outside the basal plane. Kohler[9] shows that in this instance the thermopower as a function of angle as defined in Figure 2-2 is:

$$S(\theta) = S_{\perp}\cos^2\theta + S_{\parallel}\sin^2\theta + \frac{\left(\frac{\Lambda_{\perp}}{\Lambda_{\parallel}} - 1\right)\left(S_{\parallel} - S_{\perp}\right)}{\cos^2\theta + \frac{\Lambda_{\perp}}{\Lambda_{\parallel}}\sin^2\theta}\cos^2\theta\sin^2\theta \qquad 2\text{-X}$$

$\Lambda_{\perp}$ and $\Lambda_{\parallel}$ are the two independent elements of the thermal conductivity tensor. In general the additive term is but a small correction. This is not to say that equation 2-X has not had ample experimental verification[10].

The expression given in 2-IX is often referred to as the isothermal thermopower, whereas that in 2-X is called the adiabatic thermopower.

B. The Diffusion Term

In non-magnetic materials, the thermopower may be split[11] into two terms, a diffusion term S_d and a phonon drag term S_g:

$$\underline{\underline{S}}_{total} = \underline{\underline{S}}_d + \underline{\underline{S}}_g \qquad 2\text{-XI}$$

Briefly, the diffusion part arises from the dynamic balance established between the two driving forces in the Boltzmann equation, the temperature gradient ∇T and the electric field $\underline{E}$. The rate of change of this electric field with respect to temperature is proportional to the diffusion thermopower.

An expression originally derived by Mott[12] is presented here[13] in a form applicable to anisotropic metals. The derivation depends on the Boltzmann equation in the relaxation time approximation.

$$(S_d)_{ij} = -\frac{\pi^2 k^2 T}{3|e|}\ \rho_{i\ell}\left(\frac{\partial \sigma_{\ell j}(E)}{\partial E}\right)_{E_f}$$

$(S_d)_{ij}$, $\rho_{i\ell}$, $\sigma_{\ell j}$ indicate tensor components of the diffusion thermopower, the electrical resistivity, and the electrical conductivity. k is Boltzmann's constant, T the absolute temperature and e the electronic charge. E is the energy and E_f the fermi energy. Note that the repeated index ℓ is summed over the applicable range.

For cubic metals the tensors degenerate into scalers.

For a free electron model this equation then predicts a negative thermopower with a linear dependence on the temperature. This behavior is rarely observed because of the complexity of the bracketed term even in the simple monovalent alkali and noble metals. For an anisotropic metal with a Fermi surface of many sheets the evaluation of the bracketed term becomes prohibitively difficult. We, therefore, do not intend to consider this term in detail. In undertaking this work, however, we assumed in analogy with the group 1 metals that the thermopower would be a monotonically increasing or decreasing function of T, the sign of which could be determined at high temperatures where the phonon drag contribution is expected to become small. However, recently Colquitt[14] has performed theory calculations which suggest that it may be possible to obtain maxima and minima in the low temperature thermopower of ametal which has a Fermi surface of many sheets.

C. Phonon Drag

The second term in the right hand side of equation 2-XI represents a contribution to the thermopower that results from interactions between non-equilibrium phonon distribution and conduction electrons. Phonon-electron collisions result in net changes in the velocity of the electrons involved, thus altering the electric field set up by the diffusion process. We believe that effects of this sort play the dominant role at low temperatures ($\lesssim \frac{\theta_D}{10}$, say) giving rise

to complicated temperature dependence.

Phonon drag as a possible mechanism was first suggested by Gurevich[15] in 1945. MacDonald[16] has considered the problem in a simple way and arrives at the following expressions:

$$S_g \approx \frac{C_p}{Nq} \frac{\tau_2}{\tau_1+\tau_2} \qquad \text{2-XIII}$$

where C_p is the lattice specific heat at constant pressure, N the number of changes/inner volume, q the change of the carriers, $1/\tau_2$ the "rate of momentum transfer to the free carriers", and $1/\tau_1$ the "rate of transfer for all other mechanisms (phonon-phonon, phonon-impurity, etc.)".

MacDonald analyzes this equation into two regions, above Θ_D and below Θ_D. His result is:

$$S_g \approx \frac{k}{nq\tau_1} \frac{A}{T}, \quad T > \Theta_D$$

$$S_g \approx \frac{200k}{nq} \left(\frac{T}{\Theta_D}\right)^3, \quad T < \Theta_D \qquad \text{2-XIV}$$

Here k is the Boltzmann constant, n the number of free changes/atom, A the lattice thermal conductivity, and Θ_D the Debye temperature. These results depend on the free electron model, a relaxation time Boltzmann equation.

Using a variational method, Ziman[17] arrives at a result involving specific reference to the scattering processes through (scattering operators).

Ziman's expressions are:

$$S_g = \frac{k}{q}\frac{1}{n}\frac{-P_{iL}}{P_{ll}}, \quad T > \Theta_D$$

$$S_g = \frac{k}{q}\frac{1}{n}\frac{4\pi^4}{5}\left(\frac{T}{\Theta_D}\right)^3\frac{-P_{iL}}{P_{LL}} \quad T < \Theta_D \qquad \text{2-XV}$$

The P_{ij}'s are Ziman's "scattering operators" and have the following form[18]

$$P = \frac{1}{kT}\iiint(\phi_{\underline{k}} - \phi_{\underline{k}'})\,\mathcal{J}^{\underline{k}'}_{\underline{kq}}\,d\underline{k}\,d\underline{q}\,d\underline{k}'$$

$$-P_{iL} = \frac{1}{kT}\iiint(\phi_{\underline{k}} - \phi_{\underline{k}'})\,\phi_{\underline{q}}\,\mathcal{J}^{\underline{k}'}_{\underline{kq}}\,d\underline{k}\,d\underline{q}\,d\underline{k}' \qquad \text{2-XVI}$$

$$P_{LL} \approx \frac{1}{kT}\iiint(\phi_q)^2\,\mathcal{J}^{\underline{k}'}_{\underline{kq}}\,d\underline{k}\,d\underline{q}\,d\underline{k}'$$

The ϕ's are the variational trial functions and the $\mathcal{J}$'s are the equilibrium transition rates for the scattering processes envisioned.

Simple assumptions regardingthe P_{ij}'s lead one back to expressions like equations 2-XIV. What is observed in experiment, however, seldom looks much like anything one can calculate from these equations. For example, the negative bump at low temperatures in Pb is attributed to phonon drag, whereas 2-XIV gives positive phonon drag components.

The next approximation involves looking a little harder at equations 2-XVI, and using more realistic trial functions.

Ziman[19] now inserts for the ϕ's the following expression:

$$\phi_{\underline{k}} = \frac{\tau_k}{\tau_e} \frac{m}{\hbar} \underline{v}_{\underline{k}} \cdot \underline{u}$$

$$\phi_{\underline{q}} = \frac{\tau_k}{\tau_L} \underline{q} \cdot \underline{u} \qquad \text{2-XVII}$$

τ_e and τ_L are average relaxation times construed to make the old kinetic formulae:

$$\sigma_e = \frac{nN}{m} e^2 \tau_e \qquad \text{and}$$

$$\kappa_L = \frac{1}{3} C_L u_L^2 \tau_L$$

give the actual ideal electrical and thermal conductivities. The new τ's are the true $\underline{k}$ and $\underline{q}$ dependent quantities presumably required in any detailed theory.

The result of inserting 2-XVII into 2-XVI is, of course, calamitous. There is, however, something to save the crew's drowning. Note that P_{iL} will contain a factor not unlike the following:

$$\xi^{\underline{q}}_{\underline{kk}'} = \tau_{\underline{q}} \underline{q} \cdot (\tau_{\underline{k}'} \underline{v}_{\underline{k}'} - \tau_{\underline{k}} \underline{v}_{\underline{k}}) \qquad \text{2-XVIII}$$

We note that such a factor could cause the resultant thermopower to be of either sign depending on the relevant band structure and fermi surface geometry. We shall return to

this again.

The above results, although complicated, are not yet detailed enough to describe a real metal. They do not take account of phonon dispersion or of the complex band structure and fermi surface topology found in the oscillatory experiments.

D. The Bailyn Equation

Bailyn[20,21,22] has derived an expression for the phonon drag thermopower which does allow for these facts.

$$Sg = \frac{1}{3|e|}\left(\frac{m}{N}\right)_{eff.} \sum_{\underline{q}j} \frac{dN_{oj}}{dT} \nabla\omega \cdot \sum_{\underline{k}\underline{k}'\ell\ell'}^{[\underline{q}j]} \alpha(j\underline{q};\underline{k}\ell,\underline{k}'\ell') \times$$

$$\times \left[\underline{v}(\ell\underline{k}) - \underline{v}(\ell'\underline{k}')\right] \qquad \text{2-XIX}$$

From the left, the various terms are:

e is the electronic charge

$$\left(\frac{m}{N}\right)_{eff.} = \frac{1}{N\Delta_o} \frac{12\pi^3\hbar}{\sum_{\ell} A(\ell\zeta)v(\ell\zeta)}$$

N is the number of atoms in the sample, Δ_o the atomic volume, $A(\ell\zeta)$ is the area of the ℓ^{th} sheet of the fermi surface, and $v(\ell\zeta)$ is the fermi velocity on the ℓ^{th} sheet. This expression becomes $\frac{m^*}{N}$ in the effective mass approximation. N_{oj} is the Bose distribution function. $\nabla\omega$ is the usual sound velocity which depends on the direction and magnitude of q and its polarization, j.

A given phonon, $\underline{q}$, may scatter from other phonons, from impurities and so forth, as well as inducing transitions of the form $(j\underline{q};\ \underline{k}\ell,\ k'\ell')$. $\alpha(j\underline{q};\ \underline{k}\ell,\ \underline{k}'\ell')$ represents the probability that the phonon $j\underline{q}$ will induce the event $(j\underline{q},\ k\ell,\ k'\ell')$ relative to all the other scattering events

open to $j\underline{q}$. The interested reader is referred to reference (20,21) for explicit expressions.

Finally, $\underline{v}(\ell\underline{k})$ is the velocity of the electron on the ℓ^{th} sheet.

Unfortunately, even this detailed expression will not serve for non-cubic materials. The factor of $\frac{1}{3}$ in equation 2-XIX was introduced as an average over 3 cubic directions.

Shortcomings aside, the salient point is the emergence of a factor similar in form to 2-XVIII.

$$\eta^{\underline{q}j}_{kk''} = \nabla\omega \cdot \left[\underline{v}(\ell\underline{k}) - \underline{v}(\ell'\underline{k}')\right](\alpha) = \underline{S}(\underline{q}j) \cdot \left[\underline{v}(\ell\underline{k}) - \underline{v}(\ell'\underline{k}')\right](\alpha) \qquad 2\text{-XX}$$

This must be summed for all ℓk, $\ell k'$ at a given $\underline{q}$ and polarization j.

If the q and direction dependence of S, the sound velocity, may be ignored, then:

$$\eta_{kk'} = \frac{S\underline{q}}{q} \cdot \left[\underline{v}(\ell\underline{k}) - \underline{v}(\ell'\underline{k}')\right](\alpha)$$

It is this factor that fixes the sign of the resultant phonon drag component. The difficulty is that all such components must be summed up weighted by their relative probabilities. Some generalities emerge, nevertheless. Consider the event pictured in Figure 2-3.

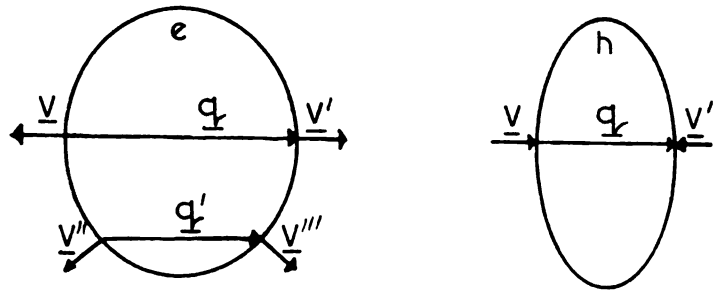

Figure 2-3

The left hand drawing represents a transition crossing a filled region in k-space. Then:

$$\underline{q} \cdot (\underline{v} - \underline{v}') = -2qv$$

But the right hand drawing which represents a transition across an empty region gives:

$$\underline{q} \cdot (\underline{v} - \underline{v}') = 2qv$$

Hence, dispersion ignored, transitions that cross filled regions contribute negative η's while those that cross unfilled regions contribute positive η's. Which sign wins out depends on the α's, and on the weighting given the $\underline{q}$'s in equation 2-XIX by the temperature derivative of the Bose distribution.

E. A Working Hypothesis

In the absence of detailed knowledge of all the factors that appear in equation 2-XIX, we appeal to a simple minded argument to gain some insight into the temperature dependence of the observed thermopower.

If one adopts a simple Debye spectrum for the lattice waves, then the number of phonons with frequency ν is:

$$N(\nu) = \frac{(\text{Const})\nu^2}{e^{\frac{h\nu}{kT}} - 1} \qquad \text{2-XXI}$$

Differentiating 2-XXI with respect to ν and setting the derivative to zero yields:

$$1 - e^{-x} = \frac{x}{2} \quad , \quad x = \frac{h\nu}{kT}$$

Graphical solution gives $x \approx 1.61$; that is:

$$h\nu_c \approx 1.61\ kT \qquad \text{2-XXII}$$

A plot of 2-XXI shows a function (figure 2-4) highly peaked at the frequency predicted by 2-XXII. What this implies is that we may define a "dominant" phonon frequency at each temperature, realizing that the Debye spectrum will obtain only at very low temperatures (say $0 - \Theta_D/100^\circ K$). Add to this the fact that the shortest wave length that is allowed to propagate in a Debye solid is[23] $(4\frac{\pi}{3})^{\frac{1}{3}}$ times

the lattice spacing: = 1.612a, which implies:

$$h\nu_{max} = k\theta_D$$

or since:

$$\nu_{max} = \frac{u}{\lambda_{min}}$$

and

$$q_{max} = \frac{2\pi}{\lambda_{min}} = \frac{2\pi}{1.612a}$$

Then:

$$\hbar u \frac{2\pi}{1.612a} = k\theta_D \qquad \text{2-XXIII}$$

Similarly 2-XXII is:

$$h\nu_c = \hbar u q_c = 1.61\ kT \qquad \text{2-XXIV}$$

Dividing 2-XXIV by 2-XXIII, we get:

$$T = \frac{q\ a\ \theta_D}{2\pi} \qquad \text{2-XXV}$$

This says that as the temperature is raised phonons of larger and larger q-vector become available in large numbers. Looking at it in another way, a given transition involving a phonon wave vector q, will have a high probability of occurring at a temperature given by 2-XXV.

We have used an extremely crude model for our phonons, and therefore must not expect much in the way of correlation with experimental results. Furthermore, the phonon spectrum is not delta-function like at q_c, but rather contains all q's up to q_c and many above (up to the cut off necessitated by Θ_D). Hence, one would expect from such a model a monotonically increasing (or decreasing contribution from each piece of the Fermi surface somewhere in the vicinity of the temperature predicted by 2-XXV.

Further smearing out of such an effect may be envisioned from the transition ($\underline{q}'$; $\underline{v}''$, $\underline{v}'''$) in figure 2-3, left. We expect the large angle scattering to give the largest contribution, but there are many such small angle events possible even with vanishingly small q-vectors. At some point, however, phonon-phonon interactions will come into play and tend to reduce α in 2-XIX to the point where phonon drag effects will essentially disappear.

F. Thermal Conductivity

Thermodynamics

The thermal conductivity tensor is defined in the following way:

$$\underline{P} = \underline{\underline{\kappa}} \cdot \nabla T \qquad \text{2-XXVI}$$

where $\underline{P}$ is the power or heat energy per unit time transmitted through the sample, $\underline{\underline{\kappa}}$ is the thermal conductivity tensor, and T is the absolute temperature.

In the hexagonal system, $\underline{\underline{\kappa}}$ has the form:

$$\underline{\underline{\kappa}} = \begin{Bmatrix} \kappa_\perp & 0 & 0 \\ 0 & \kappa_\perp & 0 \\ 0 & 0 & \kappa_\parallel \end{Bmatrix}$$

so that along symmetry directions 2-XXVI reduces to:

$$P = \kappa_i \frac{dT}{dX_i}$$

where i refers to $\perp$ or $\parallel$.

Temperature Dependence

The Free electron - Debye Spectrum result for the thermal resistivity at low temperatures ($W = 1/\kappa$) is[24]:

$$W = \frac{A}{T} + BT^2 \qquad \text{2-XXVIII}$$

where $\frac{A}{T}$ is the contribution due to impurity scattering, and the BT^2 term results from phonon-electron scattering.

Equation 2-XXVIII is the electronic part of the thermal conductivity and is the dominant factor in pure metals. It predicts a sharp rise in the thermal conductivity at lowest temperatures and then a gradual fall off at higher temperatures.

At higher temperatures 2-XXVIII predicts a rise in κ, but more complicated treatments allowing for U-processes can give a temperature independent conductivity.

From another point of view, if the Wiedemann-Franz law is valid, then κ will go like the electrical resistivity over T. Since the resistivity goes like T, κ is constant.

3. Sample Preparation

A. Generalities

Preliminary experiments indicated that sample dimensions on the order of three inches length by 0.1 inch diameter would yield thermal voltages of sufficient size to give reliable measurements of the thermopower. At the same time, it was hoped that this geometry would suffice for measuring thermal conductivities, at least in cases where this parameter is not inordinately large.

Most of the samples were cut from commercially obtained single crystal rods. Initially, attempts were made to grow large single crystals of Cadmium in a Bridgmann furnace. We found that while relatively thin, long crystals of random orientation were easily grown, attempts to increase the diameter above 1/8 inch resulted in multicrystalline blocks.

Since it is necessary to have samples that are oriented in specific symmetry directions relative to the sample axis, it becomes necessary either to seed small crystals in the desired orientation or to cut the sample of the required orientation from a large block. Seeding in a vertical Bridgmann furnace is at its best a black art and large monocrystals seemed out of the question. The commercial firm* from which one of the zinc crystals was obtained ran into the same troubles with Cadmium we encountered.

---

*Alfa Inorganics, 6 Congress Street, Beverly, Massachusetts

We anticipated the same sort of difficulties with Zinc and Magnesium. In addition, Magnesium attacks glass. Since crucibles containing the stock material are usually sealed off under vacuum in glass, this difficulty becomes prohibitive.

In the end, however, we did come upon a method of growing Cadmium crystals. The method employed is discussed in section 3-B below.

B. The Growth of Cadmium Crystals

Both Cadmium crystals were grown in our laboratories using a horizontal zone technique developed by J. C. Abele. Heat to produce the zone was provided by a movie projection bulb mounted at one focal point in an elliptical reflector.* The sample is then located at the other focus of the ellipse, resulting in a highly concentrated and confined spot of radient energy. The molten zone was easily controlled by adjusting the lamp voltage with a variac.

Crystals were grown in this apparatus in two steps. Pellets of "69" Cadmium** were first etched in a solution consisting of 3 parts nitric acid and 1 part glycerine and rinsed in double distilled water. A boat was made of spectroscopic carbon rod and etched in aqua regia. After rinsing in distilled water the boat was baked and then outgassed under vacuum. The shot was placed in this boat and

---

*Source: Materials Research Corp., Route 303, Orangeburg, N.Y.

**Source: Cominco American, Inc., Spokane, Washington

the combination was outgassed, backfilled with ~ 10.0 cm of hydrogen to produce a reducing atomosphere, and sealed off in cleaned pyrex tubing. The shot were then melted together in the horizontal zone apparatus and the resulting bar removed from the pyrex and etched again to remove the surface slag. An inch or so was removed from one end to make room for the seed and the bar re-etched.

Having prepared the seed (see below), it was placed in the boat together with the rod. This was again sealed off in a hydrogen atomosphere and positioned on the cart. The lamp was adjusted to produce a small zone ($\frac{1}{2}$ - 1 inch) in the rod at some distance from the seed. By moving the cart the zone was inched up to the seed and finally advanced part way into it. The cart drive was reversed and the zone allowed to proceed to the other end of the boat. In this way the entire rod was caused to grow in a single crystal oriented in the direction of the seed. The end product was about 3/8" in diameter and 5" long.

The Seed

The seed was produced in the same way, but in this case a molten zone was allowed to proceed slowly down the bar by pulling the pyrex tube past the lamp in a cart by means of a variable speed motor. By chance the first such attempt produced a single crystal only a few degrees from the basal plane. A two inch section was spark cut from the bar, oriented by means of a back reflection Laue camera, and spark cut along a direction in the basal plane with a

tool made of 3/16 inch thinwall stainless tubing.

This technique is highly recommended as a source of excellent quality single crystals of materials with melting points below 1000°C. At first glance, however, one might think that low melting point metals like Cadmium that have high vapor pressures would tend to plate out on the glass tube, thus preventing light from entering the sample container. In actual practice the lamp merely vaporizes the plated metal and all proceeds as desired.

C. Orientation and Shaping

The single crystal rods were oriented by the Laue method and transferred to a Servomet spark cutter. This procedure was capable of producing specimens with orientations within 1 to 3 degrees of the desired direction.

Long, thin, cylindrical samples were cut (with the exception of $Zn_{||}$ for which a long tube was used) with a tool like that shown schematically in figure 3-1.

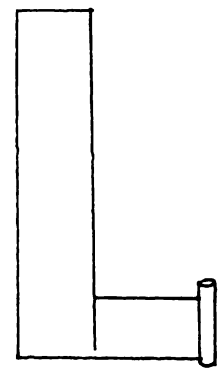

Figure 3-1

The actual cutting was done by a small length of 1/8" x .010 wall stainless steel tubing. This arrangement gave the most uniform cross sections and took the least amount of cutting time. The resultant physical dimensions are given in Table 3-1 with reference to Figure 3-2 below.

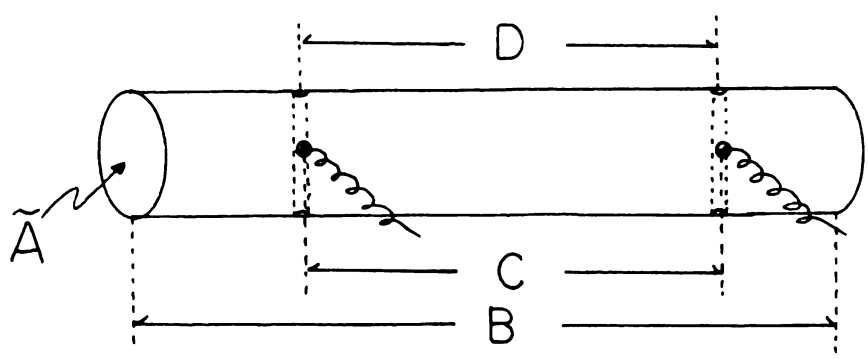

Figure 3-2

$\tilde{A}$ is the average cross-sectional area as determined by actual micrometer measurements and by weight. The later procedure consisted of weighing the sample, measuring its overall length (B in Figure 3-2 and Table 3-1) and calculating the area from the known densities of the metals used.

In order to ensure that no significant temperature gradients appeared at the differential thermocouple - sample interface, holes were spark cut using 18 gauge copper wire

	Source	Purity	R.R.R.	DIMENSIONS			
				A (cm^2)	B (cm)	C (cm)	D (cm)
Cd	M.S.U.	"69"	24,000	.0453	6.80	4.56	4.59
	M.S.U.	"69"	44,000	.0501	6.096	5.029	5.055
Zn	Alfa Inorganics	"69"	2,600	.0466	7.391	4.928	4.928
	R.C.I.	"59"	15,000	.0469	5.59	4.39	4.19
Mg	Aremco	"49"	24	.0483	6.98	4.37	4.34
	Aremco	"49"	65	.0509	6.60	4.242	4.293

Table 3-1

as the tool, and the thermocouples firmly varnished inside after having been insulated with cigarette paper. The distance between these holes is shown as "D".

Also included in these tabulations is the distance between the two soldered potential probes, C.

D. Sample Purity

Included in Table 3-1 are the sources and purities of the crystals used. In this case purity refers to the quoted purity of the starting materials. The firms mentioned are Alfa Inorganics, 6 Congress Street, Beverly, Massachusetts; Research Crystals, Incorporated, Richmond, Virginia; and Aremco Products, Briarcliff Manor, New York. The entries, "M.S.U." refer to crystals grown in our laboratories.

We also measured the Residual Resistivity Ratios of all the samples. This term is defined below:

$$R.R.R. = \frac{\rho_{297^{\circ}K}}{\rho_{4.2^{\circ}K}}$$

and is a measure of the purity and state of anneal of a given metal, ie. the higher R.R.R., the more perfect the metal crystal.

Since the thermopower of a pure metal is extremely sensitive to impurity content, the necessity of having clean samples is apparent. We now feel that considerably better samples could have been grown in the cases of $Zn_{\perp}$ and both

Magnesiums using the horizontal lamp technique used for the Cd crystals.

Whether or not significant, it is interesting to note that in each case the perpendicular sample had a lower R.R.R. than its parallel partner.

4. Apparatus and Experimental Technique

A. Objectives

In order to measure thermopower and thermal conductivity on single crystals, one must introduce and measure a thermal gradient along the sample, measure the power required to produce each gradient, and finally measure the electrical potential difference generated by the gradient. To obtain these coefficients as functions of temperature, it is necessary to have some scheme of changing and accurately monitoring the sample temperature. How these requirements were met is the topic of this section.

B. The Cryostat

The cryostat used in these measurements consists of two concentric cylindrical vacuum cans, suspended by cupro nickel tubes from a brass flange at the dewar head, with an arrangement for controlling the pressure in each one independent of the other (Fig. 4-1). The inner can is always evacuated to pressures of the order of 5×10^{-6} mm of Hg, thus eliminating the possible source of error in K due to convection heat exchange and, at the same time, minimizing the heat required to maintain the necessary temperature gradient for thermopower measurements. The space between the two cans may be held at any convenient pressure ranging from hard vacuum (5×10^{-6} mm) when the inner can is maintained at a high temperature relative to the working bath, to 1 atmosphere during precool. This arrangement provides a simple means of obtaining a controlled heat leak between the sample holder and the bath. It is therefore possible to work at

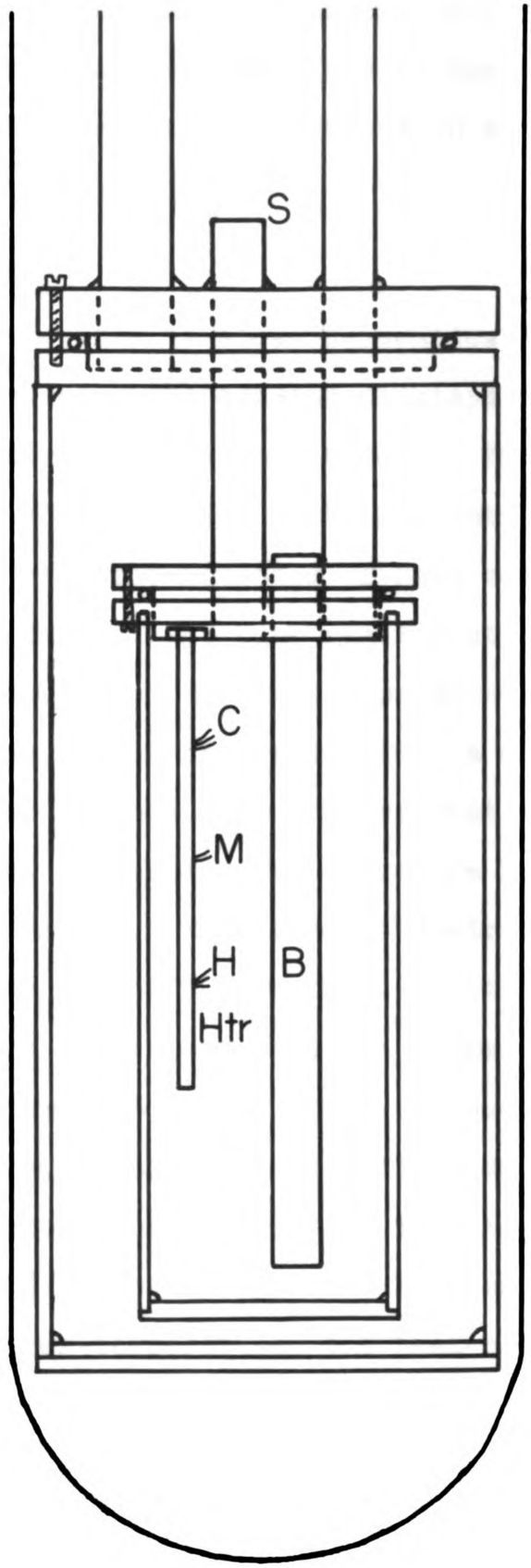

Fig. 4-1

temperatures near the bath, an otherwise difficult feat in view of the rather large quantities of heat involved in producing sizeable temperature gradients in samples of high thermal conductivity.

The Vacuum System:

The vacuum system is shown schematically in Figure 4-2. The left hand side of the drawing displays the high vacuum section which serves the sample holder. The method for introducing controlled quantities of He gas into the space between the two vacuum cans for purposes of heat exchange is shown at the top left. The ballast tank remains at approximately 1 atmosphere absolute and He at this pressure is admitted by means of a 3-way vacuum ball valve into a short stub. The gas in this stub expands into the cryostat to a final pressure of ~ 25 microns. Repeating the procedure builds up the exchange gas pressure. When less is desired, some may be pumped away with the diffusion pump. In this fashion the heat leak may be varied over quite a range of values. This is important between 5 - 30^{o}K where the sample conductivity becomes high, requiring large quantities of heat to produce a measurable temperature gradient. This heat must go somewhere (the bath) or the sample will heat as the gradient is raised. At higher temperatures the heat capacity of the inner can as well as radiative heat transfer become large enough to accomodate the impressed heat. In addition, the cupro nickel tubes contribute to the required heat leak.

The situation is somewhat similar in the range from 78 - 85°K with LN_2 as cryogen. Generally 200-300 μ of He* gas is required to hold 78°K in the course of a measurement.

Even with several hundred microns of exchange gas present, reliable data below 6 or 7°K was hard to collect. A rather larger heat leak in the form of a wire, perhaps, would be required to take measurements in this region.

It was partly for this reason that it was decided to attempt measurements at 4.2°K and below. To achieve this, the outer can was removed, thus placing the OFHC** copper flange of the inner can directly in contact with the He bath. The vacuum arrangements for achieving reduced temperatures are shown on the R.H.S. of Figure 4-2. A Walker manostat is used to control the pressure over the He bath. The vapor pressure of the bath is read on a mercury manometer, and at lowest pressures, a McCleod gage. These pressures were converted to temperatures by the 1958 He temperature scale.

During the course of these measurements, a gaseous He recovery system was installed in our laboratories. Hence provisions are shown for returning boil-off to the central collection bag.

Sample Holder:

Figure 4-1 details the sample holder utilized. The two vacuum cans are sealed with pure lead wire wrapped in a

---

* The thermal conductivity of helium is not appreciably larger at STP than at ~300μ

** OFHC: Oxygen free high conductivity

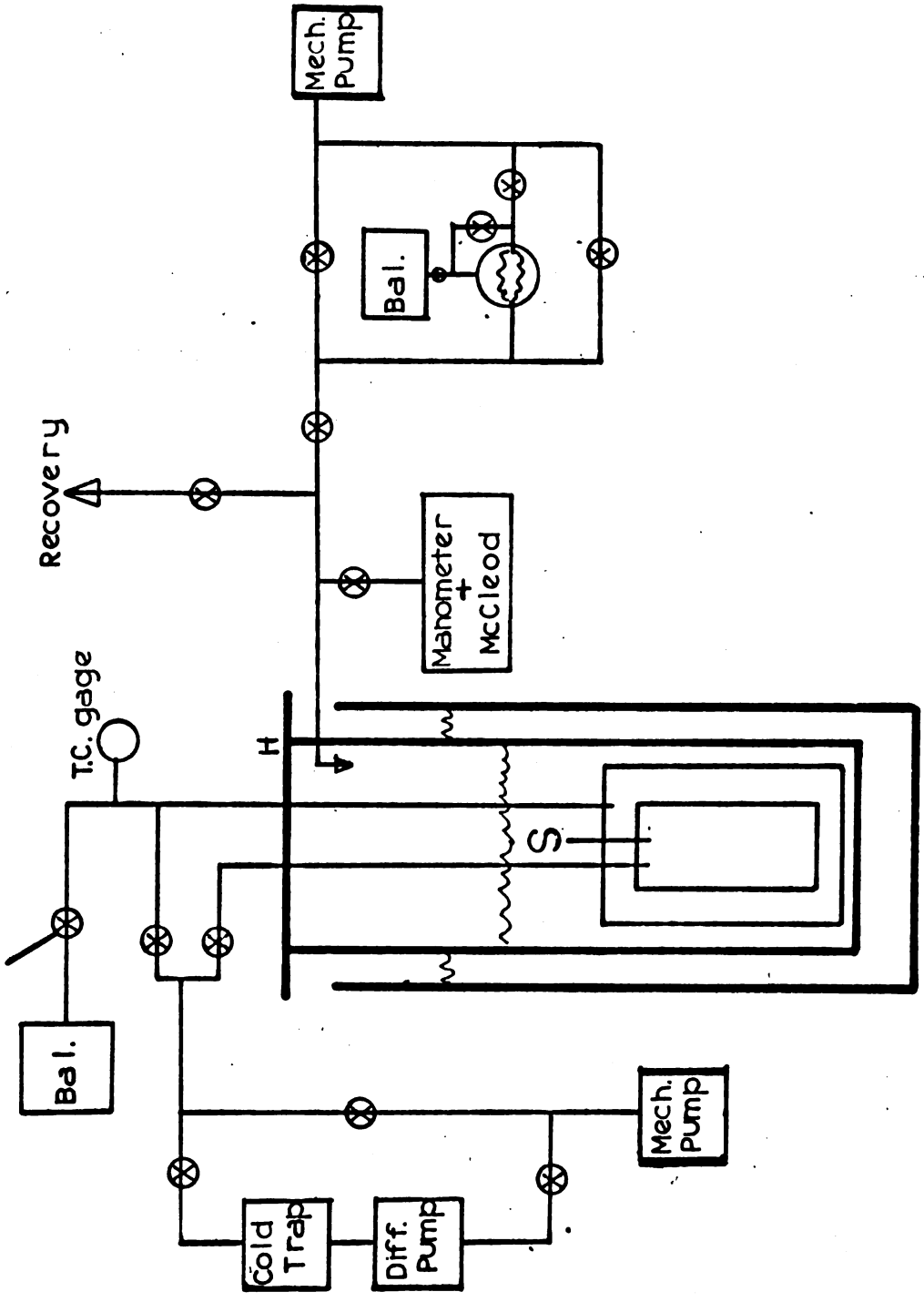
Mech. Pump
Bal.
Recovery
Manometer + McCleod
T.C. gage
H
S
Bal.
Mech. Pump
Cold Trap
Diff. Pump

FIG. 4-2

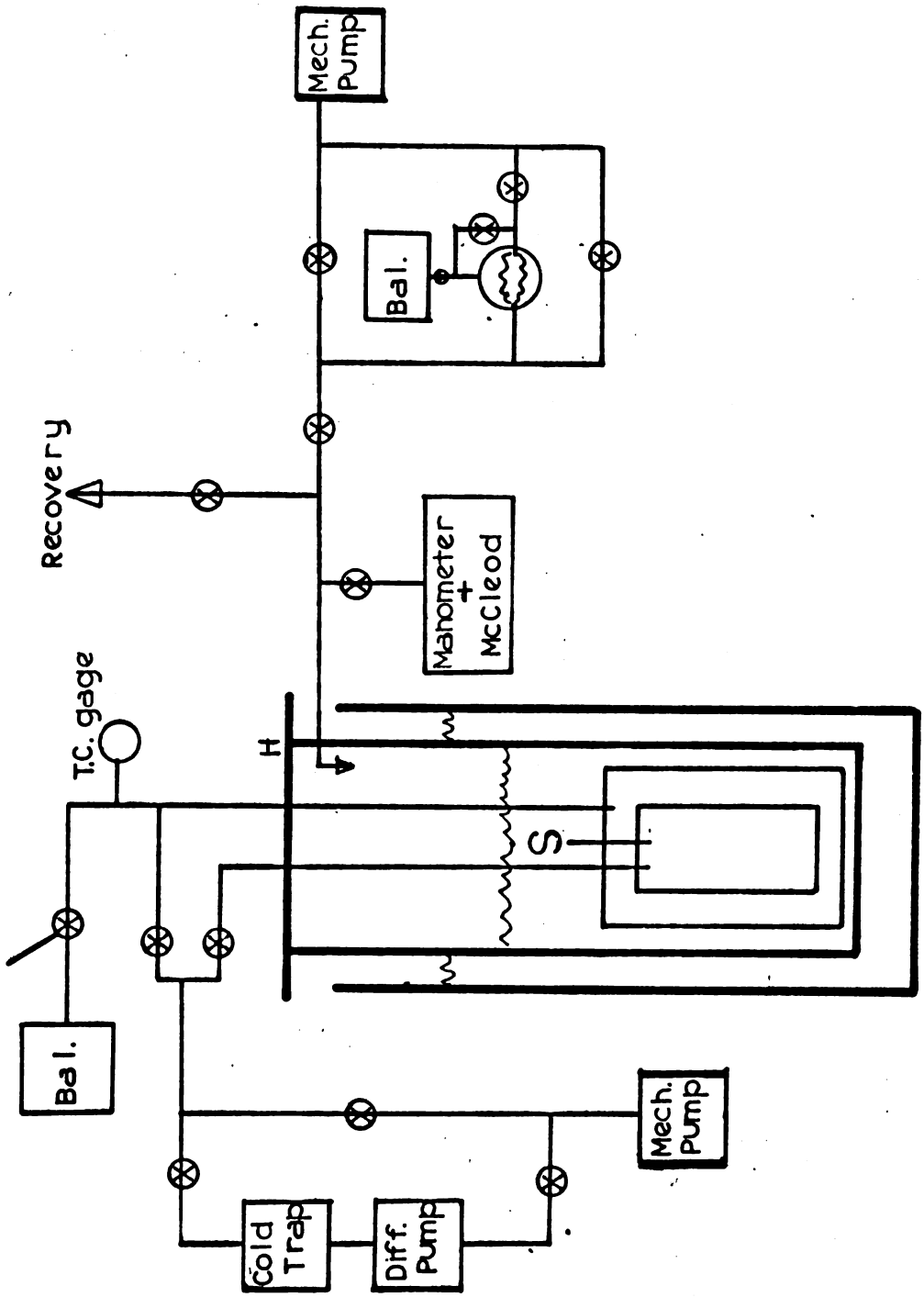
Mech. Pump
Bal.
Recovery
Manometer + McLeod
T.C. gage
H
S
Bal.
Mech. Pump
Cold Trap
Diff. Pump

FIG. 4-2

single turn around the protruding lip on the upper flanges, twisted tight and squashed by the screws shown. The lead used was 41 mill. for the outer can and 31 mill. for the inner can. Both are smeared lightly with silicone grease before installation. This apparently helps the lead flow into nicks and faults, thus insuring a good seal.

The outer can is constructed entirely of Brass and soldered together with Eutectic Solder which fuses at about 900°F. This was used so that further connections (for example, to the tube carrying the epoxy seal) could be made with soft solder.

The inner can is made of copper and assembled with the same Eutectic Solder. In particular, as previously mentioned, the flanges are made of OFHC copper. This was done to insure rapid heat transfer within the various parts of the can so that equilibrium could be quickly attained. Furthermore, when operating below 4.2°K, high conductivity Cu was deemed essential to keeping the sample's cold end at the bath temperature.

The binding post (B in Figure 4-1), similarly constructed of OFHC Cu, serves two purposes. It provides a convenient place to tie down fragile wires and, more important, it helps make sure that the various probe wires are near the temperature of the sample. This helps eliminate the chance of large temperature gradients being developed across solder joints and glue joints on the sample which might otherwise lead to measurement errors. The binding post was first

wrapped with a layer of cigarette paper and then varnished with G.E. 7031. All probe wires were then wrapped with several turns and varnished in place. This afforded good electrical isolation and, at the same time, seems to have produced the required heat sink. The samples were mounted by soldering them with indium into the Cu flange (see Appendix 4-1). This method was decided upon as affording the best thermal contact to the can. Indium melts at a sufficiently low temperature (156.4°C) to allow it to be used as a solder for the present samples and, since it can be obtained in a pure state, provides a high thermal conductance to the flange.

Mounting was accomplished by tinning the sample with In, heating the entire inner flange to the melting point of In, and then plunging the sample into the pot of now molten metal contained in the flange. The procedure outlined in Appendix 4-1 was necessitated in the case of Mg, since ordinary soldering techniques are inapplicable.

A small heater was wound on an OFHC Cu cylinder approximately 3/8" long and 1/4" diameter over a layer of cigarette paper cemented in place with G.E. 7031 varnish. This heater was in turn soldered with In to the hot end of the sample, except in the case of Mg. Here cigarette paper was cemented around the hot end of the sample itself with thinned Duco cement and a heater wound directly on this base. Details on all heaters can be found in Appendix 4-2.

Probes:

Measurement probes were attached in the following fashion. As outlined in Section 3, small holes were spark cut in the samples. Into these were placed the ΔT thermocouple probes which were first wrapped with cigarette paper and then cemented in. G.E. 7031 was used for all but Mg where acetone thinned Duco cement was employed.

Spark cut holes were used in order to accomplish a low thermal resistance from sample to probe. Temperature gradients here would, of course, be detrimental to the measurements.

Thinned Duco cement has the advantage that it dries considerably faster than G.E. 7031 varnish and thus allows a reduction in the time lapse between sample mounting and apparatus seal up. The thermal resistance of this cement appears to be low enough to suit the present purposes.

The thermocouple measuring the average temperature of the sample was wrapped with cigarette paper and glued to a spot on the sample approximately midway between the two ΔT probes ("M" in figure 4-1). Since the T probe remains at roughly the temperature of the can and since it is firmly anchored mechanically and thermally to the binding post, it is not necessary to go to such great extremes in keeping down the thermal resistance of the sample-probe junction.

Specifics and calibrations of the Gold-Iron vrs. Chromel thermocouples employed are recorded in Appendix 4-3.

The thermal emf. probes were cut from "69" 10 mill. lead wire supplied by Cominco Products, Inc., Spokane,

Washington. In all cases these probes were soldered in place with Wood's metal, using Sta-Clean flux. These joints were kept as close as possible to the spark cut holes that contained the ΔT probes. See Table 3-1 and figure 3-1 in Section 3.

Epoxy Seal:

An epoxy seal (S in figure 4-2) was employed to remove the thermocouple leads from the vacuum space into the bath, while the lead wires were encased in teflon tubing and taken directly up the inner can's pumping line where they, too, left the vacuum via an epoxy seal.

The epoxy seal that sits atop the outer can and contacts the liquid cryogen was itself the object of considerable effort. Many diverse methods were tried before a reliable scheme was developed. Several authors[25,26] have described various approaches to the feed-thru problem. Most of these were found unsatisfactory for one reason or another, usually unreliability in cycling to LHe temperatures. Wheatly's method[26] was acceptable in this respect, but seals constructed after his recipe invariably caused the fragile Gold-Iron wire to sever somewhere inside the seal.

The method adopted is similar to that described by Balain and Bergeran [25].

A small brass button was turned to fit snugly into 3/8" O.D., .010" wall stainless tubing. It was then soft soldered into a 1.3" length of the above mentioned stainless steel tubing. Finally, a 0.1" hole was drilled in the button.

The whole piece was rinsed in methanol and the thermocouple wires were passed through, leaving sufficient length extending from each end. The chromel being already enameled, no further insulation was necessary. The Gold-Iron was bare and it was left so. At this point a small batch of Stycast 2850 GT mixed with 5% by weight of catalyst No. 9* was prepared. This viscous mixture was then filled into the previously drilled hole and the result allowed to cure for 48 hours. An earlier attempt with the recommended 7% catalyst No. 11 baked at 150°C cracked after a short period of time.

The seal described has been in use for several months and has withstood thermal cycling from 1.25°K to room temperature in the course of all the measurements that were taken on this piece of apparatus. It is vacuum tight ($< 2 \times 10^{-6}$ mm) and provides extremely good electrical insulation from ground.

Once prepared, the wires were protected with teflon tubing and the end opposite the seal was soldered into a 3/8" copper coupling to join the seal to the seal line (S in figure 4-1). During soldering the seal was protected with wet tissue paper.

---

*Stycast supplied by Emerson and Cuming, Inc., Canton, Massachusetts.

C. Electronics

This section sets forth the circuitry and allied electronics used in the present measurements.

Electrical Leads:

It is necessary to bring signal leads out of the cryostat in a manner that minimizes pickup and stray thermoelectric potentials. This was accomplished by the use of extensive electrical shielding throughout and heavy heat sinking and thermal shielding, especially where joints were required.

As mentioned previously, the lead potential probe wires were run up the inner can's pumping line. They were removed from the pumping line by means of an epoxy seal at the dewar header (H in figure 4-2) and joined to copper wires by squashing the prepared Pb and Cu wires between pure copper washers. The connections and seal were encased in a heavy brass can supported above the dewar flange to prevent frosting during transfer of liquid helium. Another seal and can assembly removes copper wires that have been soldered to the thermocouple wires on a terminal strip located near the low temperature seal just above the sample holder. All these copper wires pass through one shielded braid to an aluminum box located near the instruments. This box contains a heavy terminal block constructed as follows:
A 6" x 4" x 1" slab of lucite was attached inside a 7" x 5" x 3" aluminum minibox. Twelve 1" x 1" x $\frac{1}{8}$" copper slugs were formed and drilled to make square "washers". These were secured in pairs to the lucite base with $\frac{1}{4}$" x 20" nylon bolts.

Cryostat leads are joined in this box to shielded copper wires that go directly to the various measuring instruments. The foregoing precautions were undertaken to minimize thermal voltages in the leads. A modicum of success was achieved in this regard -- ambient thermals being on the order of tenths of microvolts and relatively stable.

Measuring instruments:

Figure 4-3 shows a block diagram of the circuitry involved. From the left, the abbreviations employed stand for the following: K3 is a Leeds and Northrup type K-3 potentiometer. L&N N.D. is a Leeds and Northrup model 9834 null detector. K149 refers to a Keithley model 149 milli-microvoltmeter; K147 is a Keithley model 147 nanovolt null detector, M2D2 is a Moseley model 2D2 x-y recorder, and VTVM is a Hewlett-Packard model 410BR vacuum tube voltmeter. The boxes labelled "heater control" and "power supply" are described in detail in Appendix 4-4, and the heaters in Appendix 4-2.

The vertical string of instruments on the left was used to measure and control the average sample temperature. Output from the Gold Iron - Chromel thermocouple, whose reference is the working cryogen (liquid He or nitrogen),feeds the K3 potentiometer. Voltage unbalance between the actual thermocouple voltage and the setting on the potentiometer is detected and amplified by the model 9834 null detector. This imbalance is used to control the heater marked T-control via the heater control circuit described in Appendix 4-4.

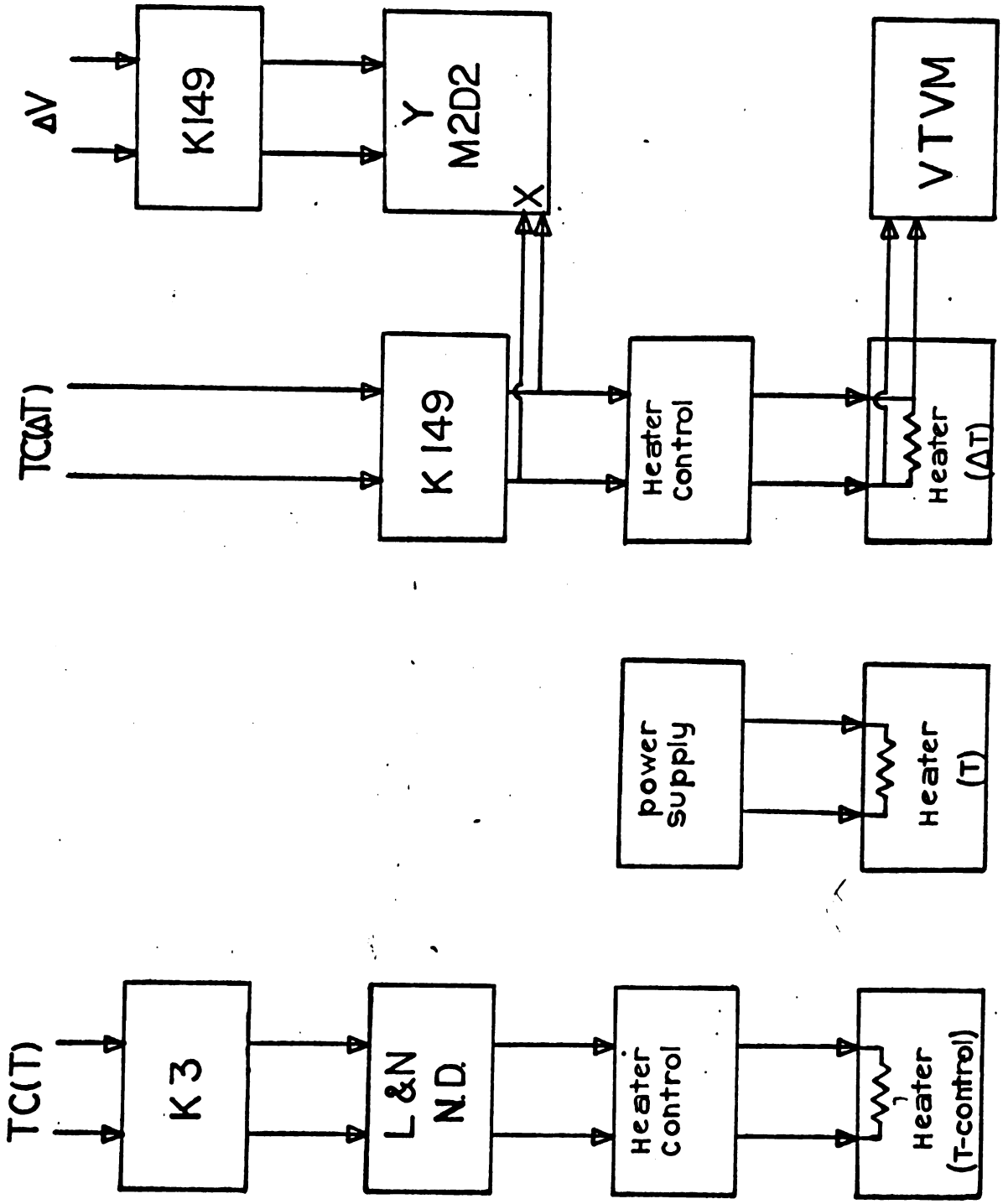
TC(T)
K3
L&N
N.D.
Heater
Control
Heater
(T-control)
power
supply
Heater
(T)
TC(ΔT)
K149
Heater
Control
Heater
(ΔT)
ΔV
K149
Y
M2D2
X
VTVM

FIG. 4-3

This arrangement allowed voltage discrimination on the order of .5 μV which corresponds to .05 K^{o} at 4.2 and .02^{o}K at room temperature. The controller generally held the sample temperature to within .1 K^{o} over the range from 4 - 300^{o}K.

The second string of blocks in figure 4-3 consists of an adjustable current source and a power heater. This combination was used to provide the gross quantities of heat required for quick temperature changes and for holding temperatures well above the bath, especially in the case of LN_2 with the sample can at 300^{o}K. In this instance rather larger quantities of heat than can conveniently be supplied by a sensitive controller were needed to maintain the high difference in temperature between the bath and the sample can.

The third string of instruments utilizes a Keithley model 149 millimicrovoltmeter to measure the output of the differential thermocouple. The output from this Keithley drives a second heater control, as described in Appendix 4-4, and the x-axis of the Moseley x-y recorder. For runs above 4^{o}K, the K149 was used in its 10μV f.s. setting, thus giving accuracies on the order of .2μV which translates to .02K^{o} at 4^{o} and .01K^{o} at 300^{o}K. Since the largest temperature gradient employed was about 0.5 K^{o}, this corresponds to 2 - 4% accuracy in the measurement of ΔT. Below 4^{o} K149 was used on either the 3μV or the 1μV f.s. setting. However, ambient noise cancels out any gain in relative accuracy.

The Keithely model 147 nanovolt null detector was used

to measure and amplify the signal from the lead potential probes. The output from this instrument drives the y-axis of the Moseley recorder. The Keithley 147 was used on various ranges depending on the relative size of the thermoelectric voltage. Ranges utilized were between .03 and 10 μV f.s. Accuracy in this leg can be expected to be 2 - 4%.

This leaves only the Hewlett Packard VTVM. It was used to measure the voltage drop across the ΔT heater, thus giving a measure of the power feed through the sample. Estimated accuracy is 3 - 5%.

D. Method of Measurement

Data were taken in three separate steps, corresponding to three temperature ranges.

The first step covered the range from room temperature (~300°K) to the boiling point of liquid nitrogen (77°K). With both vacuum cans evacuated to roughly 2×10^{-6} mm of Hg, liquid nitrogen was transferred into the inner dewar. As previously noted, considerable power was required to hold the inner can at 300°K. This power was supplied by the heaters marked (T) and (T-control) in figure 4-3. The potentiometer marked (K3) in figure 4-3 was set at the voltage corresponding to the desired temperature as read on the thermocouple calibration curve. In this manner the temperature controller provided vernier corrections to the power required to hold the desired temperature.

When the average sample temperature had stabilized, measurements were begun. With no current through the ΔT-Heater, and the remainder of the electronics activated, the point plotting mechanism of the Moseley x-y recorder was activated, thus plotting a point mark on $8\frac{1}{2}$ x 11 graph paper. This done, the ΔT heater control was advanced so as to increase the temperature gradient along the sample. Sufficient time was allowed for dynamic equilibrium to set in, and a second point was plotted. This was repeated at least four times. At each point the voltage across the ΔT heater was read and recorded. The thermal emf vrs. temperature difference points lie approximately on a straight line.

The final temperature difference varied from .5K° at high temperatures to .1K° at lowest temperatures.

When these measurements were completed, the K3 was set for the next, usually lower, temperature (say, 290°K), causing the control heater to cut off; the T-heater was turned off, and 100μ of He gas was admitted into the outer can. Exchange between the 2 cans then took over, rapidly cooling the inner can to the next point of interest. Somewhat before the next set point was reached the T-heater was turned back on and the exchange gas pumped away. After equilibrium was reestablished the procedure indicated above was repeated.

In this manner the range from 300 to 78°K was covered in 5 - 10K° steps.

The second step proceeded similarly to the first with the exception that liquid helium was utilized in order to cover the region from 80 - 6°K. The inner can was precooled to ~ 80°K along with the rest of the apparatus by admitting exchange gas into the outer can during the precool stage prior to transferring helium. The temperature of the apparatus was monitored during precool by measuring the current passed by a 1N 34A Germanium diode selected for high temperature coefficient. Once calibrated, this device could be depended upon to indicate temperatures accurately to within a few degrees at 100°K. The circuit particulars are shown in figure 4-4. Included in the same package is a bridge circuit used in conjunction with 100Ω 1/8 watt carbon resistors to sense the He liquid level. Similar devices are in wide

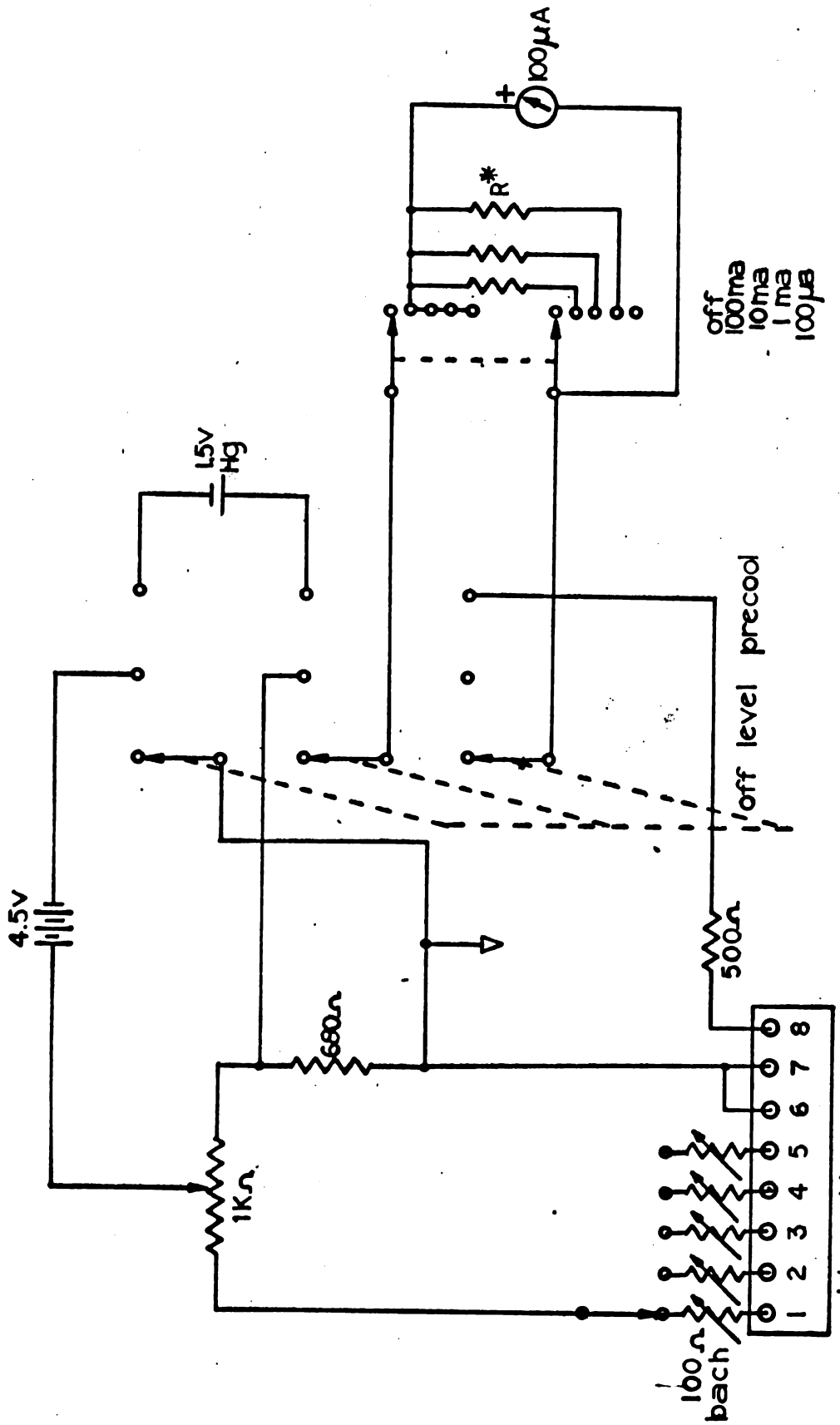
100μA
+
R*
off
100ma
10ma
1 ma
100μa
*depend on meter reading
1.5V Hg
off level precool
4.5v
500Ω
680Ω
1KΩ
blue ribbon
1 2 3 4 5 6 7 8
100Ω bach

FIG. 4-4

spread use. The prototype of this particular instrument was designed by Dr. D. J. Sellmeyer.

As in step one, measurements were initiated at an elevated temperature relative to the bath. However, upon reading 30°K the specific heat of the inner can and the various exchange mechanisms (excluding gaseous transfer) were insufficient to hold the sample temperature reasonably constant during the incrementing of the sample temperature gradient. At this point a new procedure was adopted. Some 100μ of He exchange gas was admitted to the outer can and the inner can allowed to cool to 4.2°K or so. Then by using the controller and gradually pumping the exchange gas as the set point was raised, the exchange could be carefully controlled and stable temperatures easily maintained. Overall sample temperatures in this mode could be held to something like .01°K during an entire measurement sequence. The upper limit under these circumstances was about 40°K and the lower limit 6 - 8°K, depending on the sample's thermal conductivity. This has been discussed in the cryostat section.

The last step covers the range from 4.2°K to 1.2°K. In this case the outer can was removed and the rest submerged in liquid helium. The overall temperature was then controlled by pumping on the He bath. Needless to say, the thermo-emf shrinks rapidly with temperature, necessitating a somewhat different approach. In these low temperature runs a great number of points were printed representing repeated excursions of ΔT. This resulted in a large quantity of points from which

the required slope was extracted, even though the information was masked by noise and drift. Because of the rather small voltages involved (.01 - .1 microvolts) the uncertainties are considerably larger in these low temperature data.

5. Results and Discussion

A. Data Reduction

We describe in this section the methods used to analyze the raw data taken into meaningful thermopowers and thermal conductivities.

Thermopower:

The raw data consists of plots from the Moseley x-y recorder of the sample emf vrs. the emf from the Au-Fe thermocouple measuring the temperature difference along the sample. The slope of the best straight line drawn through these points is proportional to the thermopower.

This scheme eliminates stray constant thermal emfs generated in the lead wires from the cryostat. The analysis is similar to that described below for the thermal conductivity.

However, scaling factors for the various amplifiers used and the temperature dependent sensitivity of the differential thermocouple must be taken into account. This can all be expressed by a simple equation:

$$\frac{\delta\phi}{\delta T} = (\text{scale factor}) \cdot \left(\frac{dV}{dT}\right) \cdot (\text{Slope})$$

where $\frac{\delta\phi}{\delta T}$ is the measured thermopower, "scale factor" is the ratio of Y amplification to that of X amplication in the various instruments, $\frac{dV}{dT}$ is the sensitivity of the Gold-Iron vrs. Chromel differential thermocouple*, and "slope" is the

*see Appendix 4-3

measured slope of the best fit line through the data points.

Now equation 2-VI states that we must add to the measured thermopower the thermopower of pure lead. The lead data used in this analysis is that of Christian, et al.[27]

A program was written to perform the above calculations on a CDC-3600 computer, using least squares to find the slopes. It did not produce significant improvements over the simple hand calculations in most instances and was abandoned.

Thermal Conductivity

Equation 2-XXVI says that we must measure the temperature gradient produced by a given heat flux. The latter is given by:

$$P = \frac{V^2}{R(T)}$$

where P is the power flowing, V the voltage drop across the heater, and R(T) the temperature dependent resistance of the heater. Then by 2-XXVI

$$\frac{V^2}{R(T)} = \kappa \frac{A}{\ell} \Delta T \qquad 5\text{-I}$$

ΔT is not measured directly. The measured quantity is the voltage drop across the differential thermocouple, $V_{T.C.}$, together with a thermal voltage associated with the wires coming from the cryostat. This thermal is presumed to be

constant.

ie.:

$$V_{obs.} = V_{T.C.} + \text{const.}$$

or

$$V_{T.C.} = V_{obs.} - \text{const.}$$

but

$$\Delta T = V_{T.C.} \frac{1}{dV/dT} = (V_{obs.} - \text{const.}) \frac{1}{dV/dT}$$

Substitute into 5-I:

$$V^2 = \kappa \frac{RA}{\ell} (V_{obs.}) \cdot (\frac{1}{dV/dT}) + \text{const.}$$

Hence, if V^2 is plotted against $V_{obs.}$ one should get a straight line whose slope is related to the thermal conductivity as follows:

$$\kappa = (\text{slope})(\text{scale factor})(\frac{dV}{dT})(\frac{\ell}{RA}) \qquad \text{5-II}$$

V and $V_{obs.}$ are measured at the same time as the thermopower measurements are taken. ΔT is, of course, always $<<T$ so that $\frac{dV}{dT}$ may be presumed constant. The scale factor is determined from the x-axis gain, $\frac{dV}{dT}$ is the thermometer sensitivity as before, ℓ is the distance between thermocouple junctions, R is the resistance of the heater, and A is the crossectional area of the sample. (See Table 3-1 for

measured room temperature values). The temperature dependence of the resistance wire used in the heaters is tabulated in Appendix 4-2. The data were corrected for this as well as for the anisotropic thermal contraction displayed by the present samples. The data given in reference (28,29) were used for the corrections. The overall correction is as high as 15% at low temperatures.

B. Results

Thermopower:

This section sets forth the results of our measurements of the thermopowers of Cd, Zn and Mg.

- Cadmium

Figure 5-1 shows the results of measurements performed on 2 cadmium crystals. These are to be compared with measurements taken on polycrystalline Cd wire as shown in figure 1-1. In the former data we find considerable anisotropy and a fair amount of detail especially in the parallel component.

Attempts to fit the data of Figure 5-1 to various power laws in temperature were non-productive. From this we conclude that no simple temperature dependence exists in the range we have studied.

- Zinc

Our thermoelectric measurements on zinc are shown in figure 5-2. The anisotropy in this material is even more

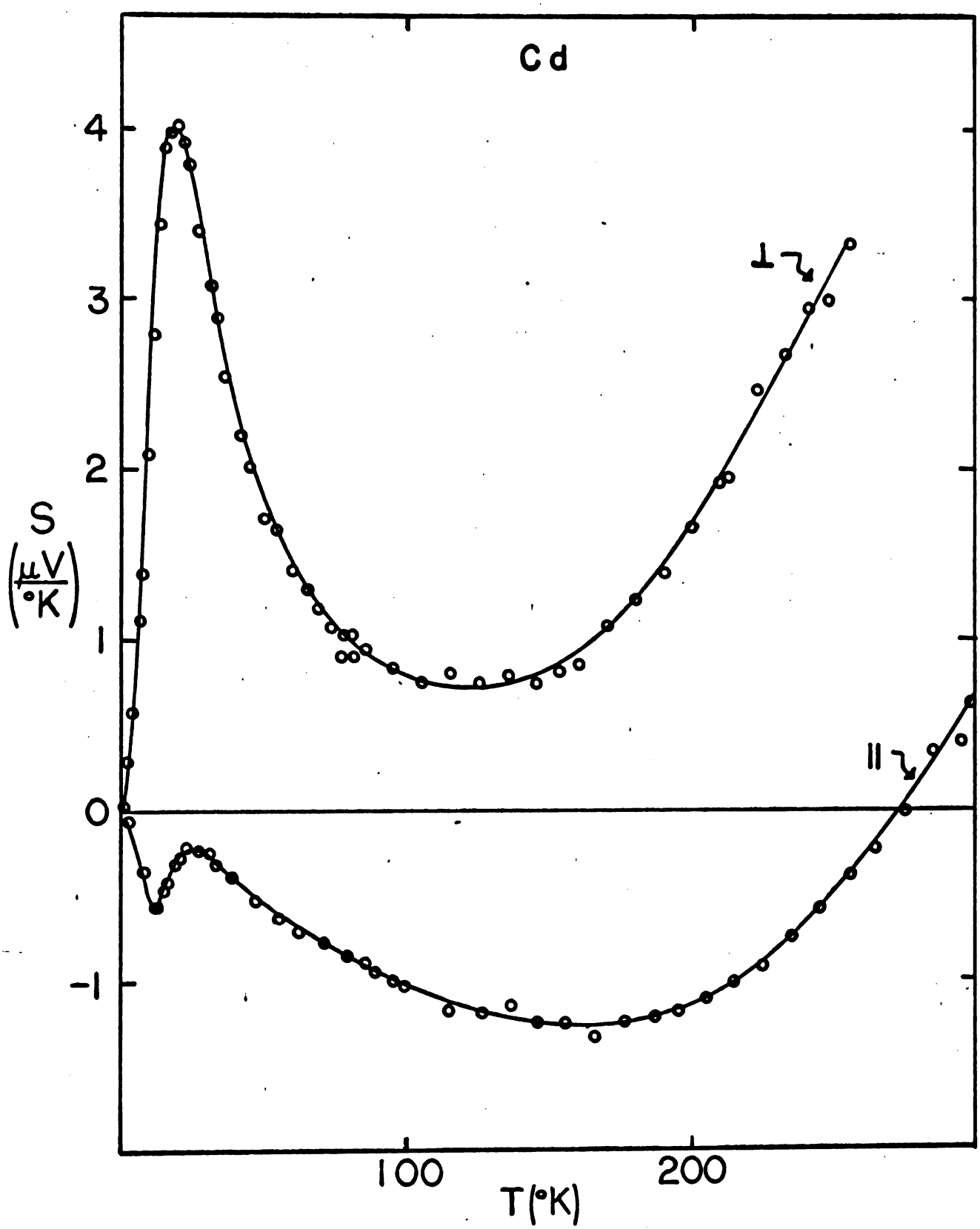

FIG 5-1

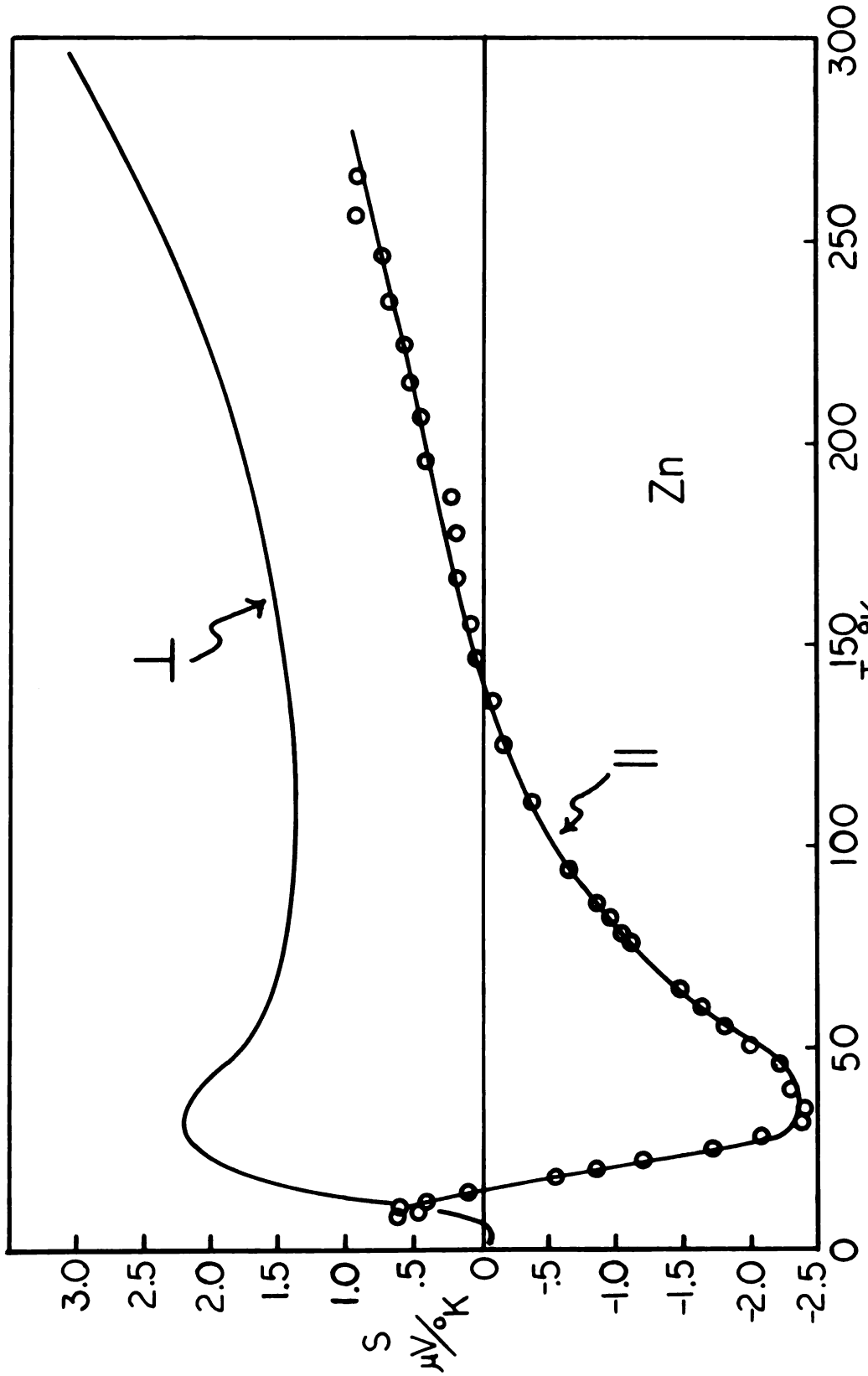

Fig. 5-2

marked than that in Cadmium.

Unfortunately, the parallel crystal fractured during the last liquid helium transfer. Hence, we have no data below 9°K and must guess at its low temperature behavior. It would appear that there is a positive peak in the vacinity of 4 degrees -- however, we have no way of defining it any more precisely.

The small negative going peak in the perpendicular component near 2.5°K is noteworthy. Together with the dip in the Cadmium parallel component, it represents unexpected detail, presumably due to complex phonon drag interactions which we discuss in detail below.

We also speculate that the relatively low R.R.R. of the perpendicular sample has depressed some of the peaks. In particular, a purer sample would probably have shown a rather larger thermopower at the peak at 30°K.

- Magnesium

Thermoelectric data taken on Magnesium single crystals are shown in figure 5-3. For comparison, figure 5-4 shows the results of measurements performed in this laboratory on polycrystalline Mg wire[30].

Figure 5-5 is an expanded graph of the results below 15°K. This figure is shown to point out the peculiar behavior of both thermopower components near 6°K. Rosenberg[31] has observed minima in the electrical resistivity and thermal conductivity at the same temperature. Presumably, this

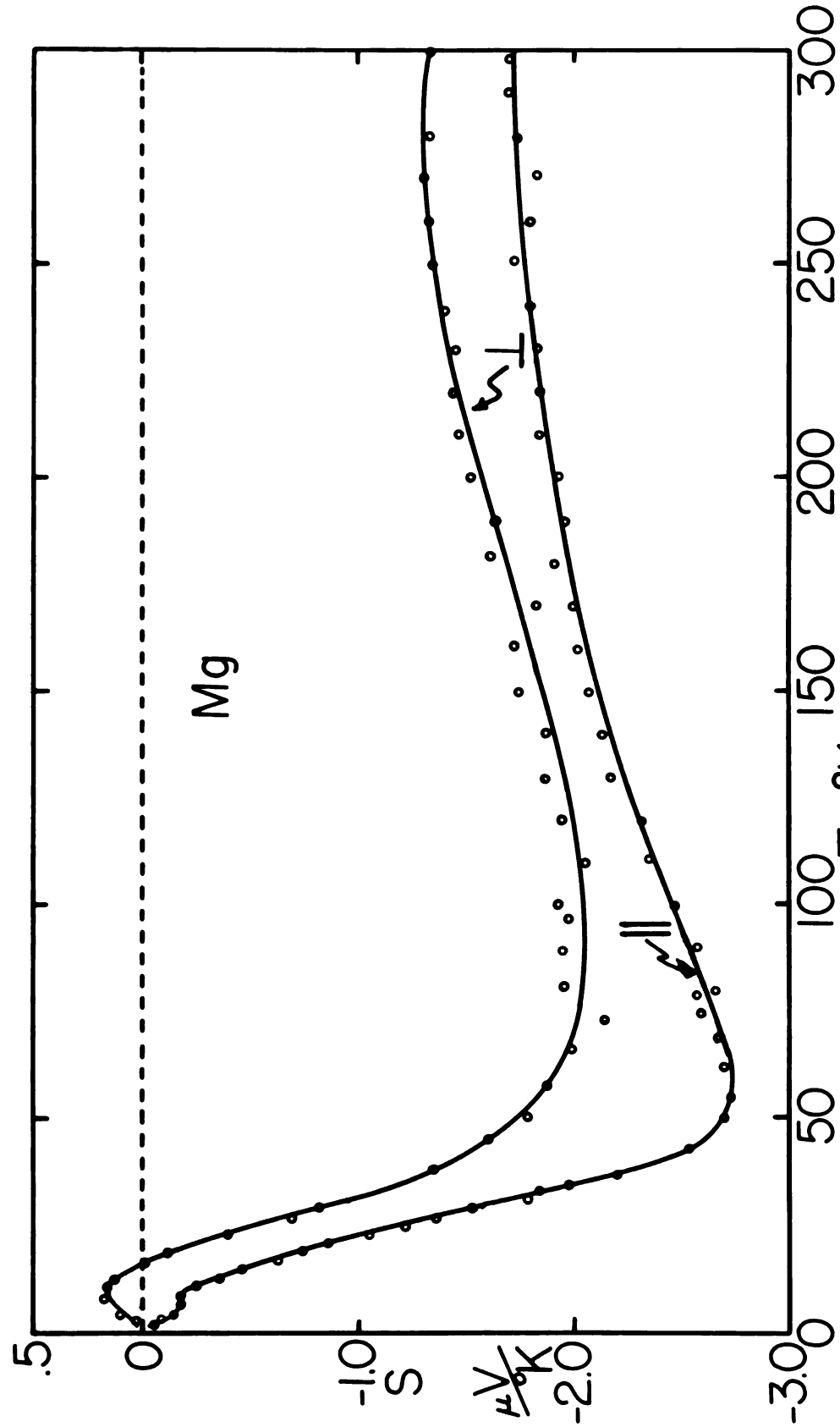

Fig. 5-3

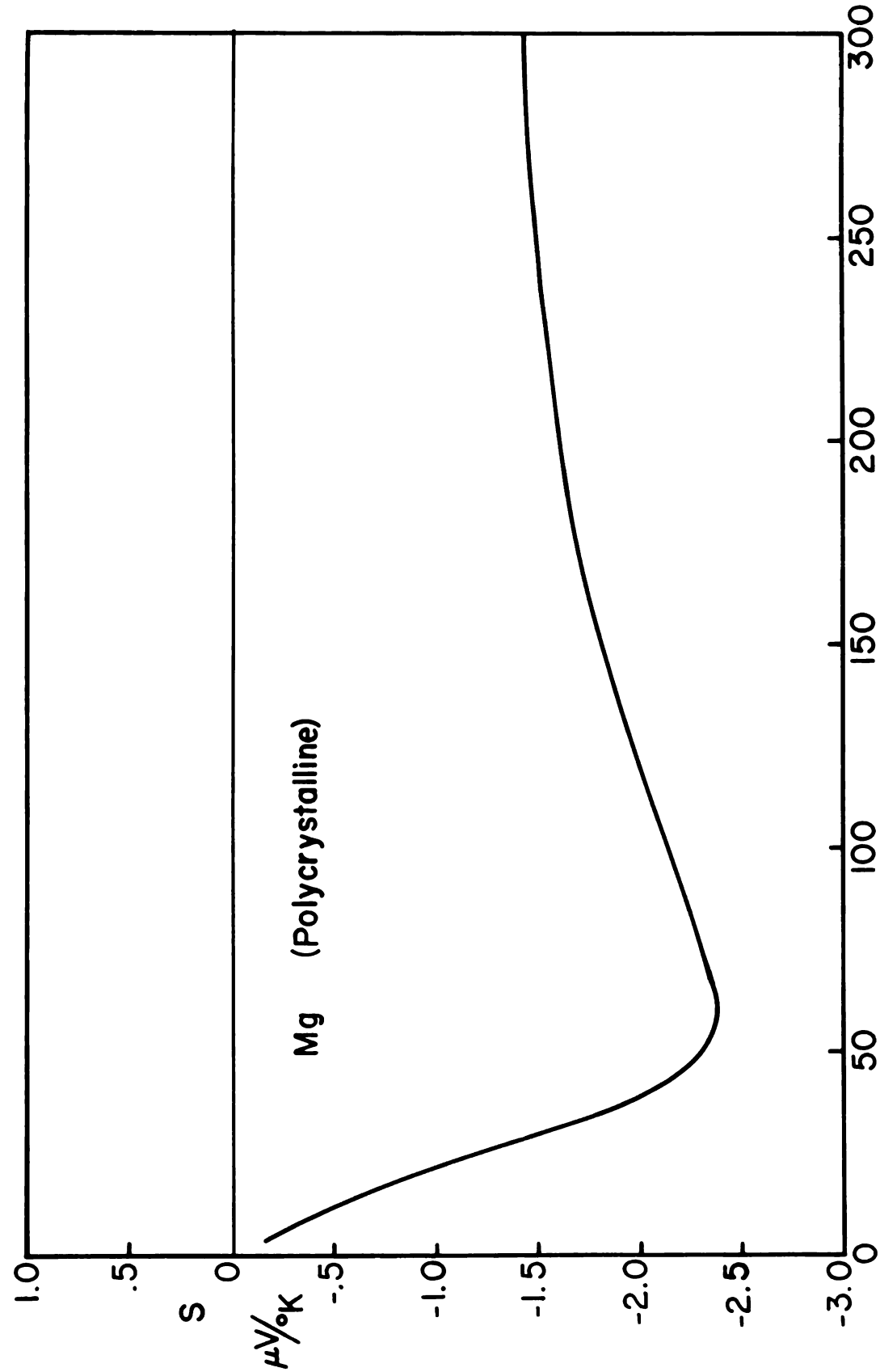
Mg (Polycrystalline)
S
μV/°K
T °K
1.0
.5
0
-.5
-1.0
-1.5
-2.0
-2.5
-3.0
0
50
100
150
200
250
300

Fig. 5-4

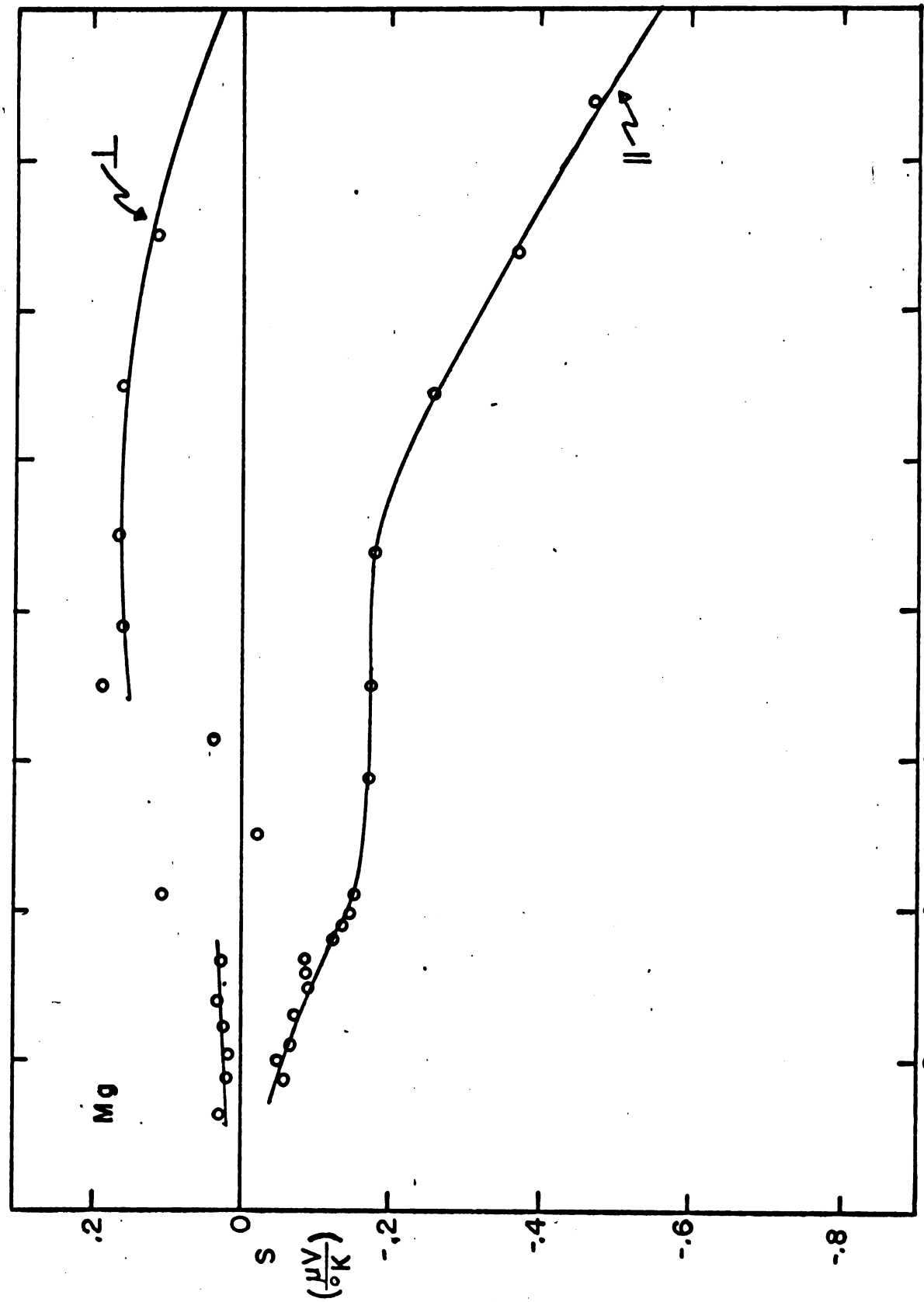

FIG 5-5

effect is similar to that in Gold and Copper, which show resistance minima in the presence of magnetic impurities like Iron.

The present results point out the difficulty of interpreting the thermopowers of polycrystalline samples of non-cubic metals. A similar remark can probably be made for all the transport coefficients.

Thermal Conductivity:

When these measurements were initiated it was hoped that by measuring the thermal conductivities of each sample we would have the parameters required to characterize the thermopower for arbitrary crystallographic direction. (See equation 2-X). However, disparit purities among the samples has vitiated any such attempt. We therefore present the data with some general remarks but necessarily devoid of detailed discussion.

- Cadmium

This purest of all the samples has the largest measured thermal conductivity as shown in figure 5-6. In fact, the conductivity was so high that our experimental set up was incapable of making reliable measurements in the near vacinity of the conductivity maxima. These fall near $6^{o}K$ in the perpendicular component and $4^{o}K$ in the parallel component. This is consistent with the expressed temperature dependence set forth in Chapter 2 and the measured R.R.R.'s.

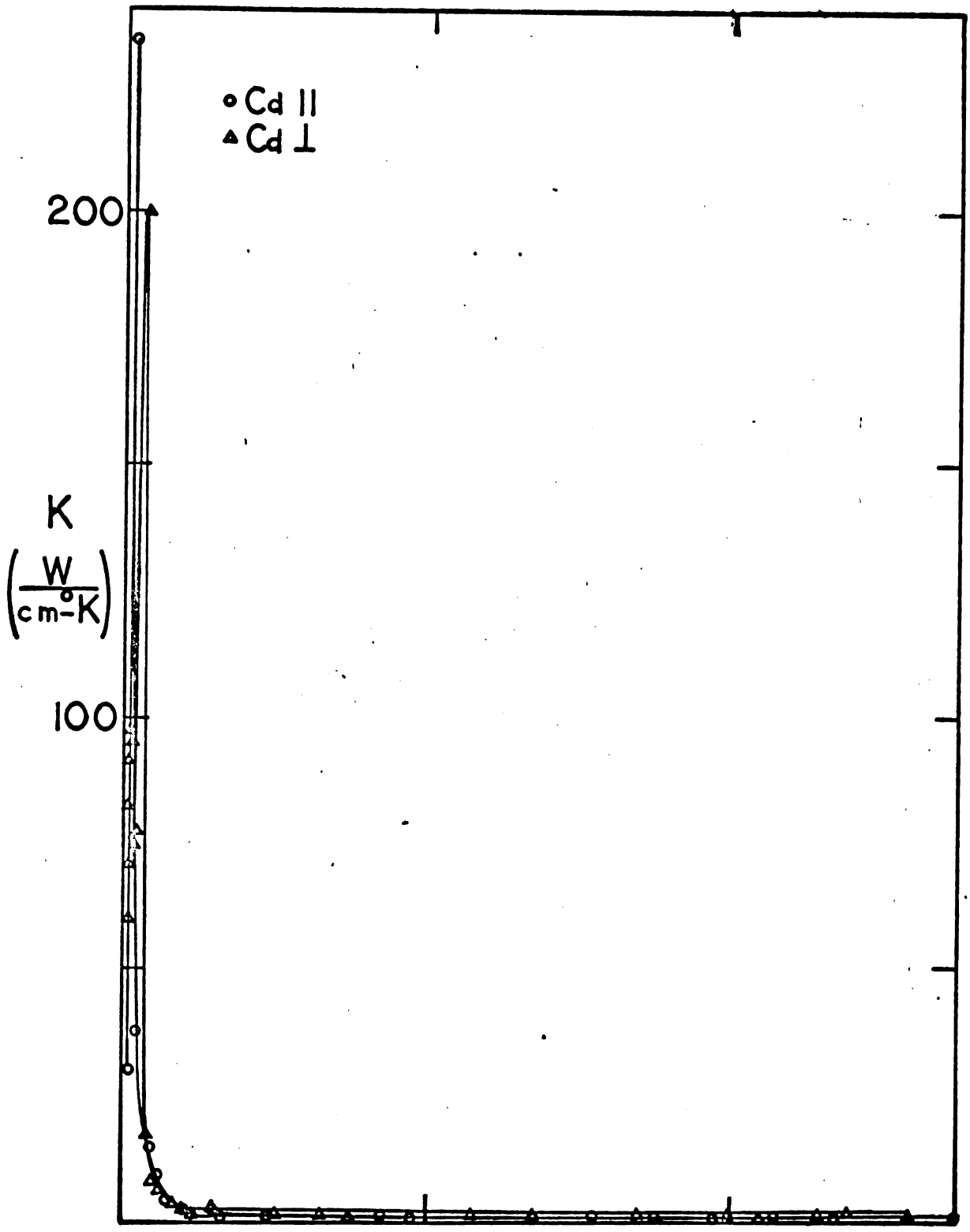

FIG 5-6

- Zinc

Figure 5-7 shows the analyzed thermal conductivity data obtained for the two symmetry directions in Zn. Here, too, the magnitude of the effect made measurements difficult. However, the data are complete enough to show generally the expected temperature dependence in the vicinity of the peak. The positions and heights of these peaks are again consistent with the R.R.R.'s.

- Magnesium

In figure 5-8 the data obtained from the two Mg samples is plotted. Ironically, the most complete data comes from the worst samples. Of course, this happens because a sample of low thermal conductivity generates a large temperature gradient for relatively small heat inputs. The difficulty with very pure samples arises from the necessity of putting large quantities of heat into the sample. This becomes a problem if the thermal contact resistance is greater than the thermal resistance of the sample. Then the sample will heat up, making it impossible to obtain measurements.

An interesting feature of the Mg data at high temperatures is its apparent increase above 120^{o}K. At this point no explanation is immanent.

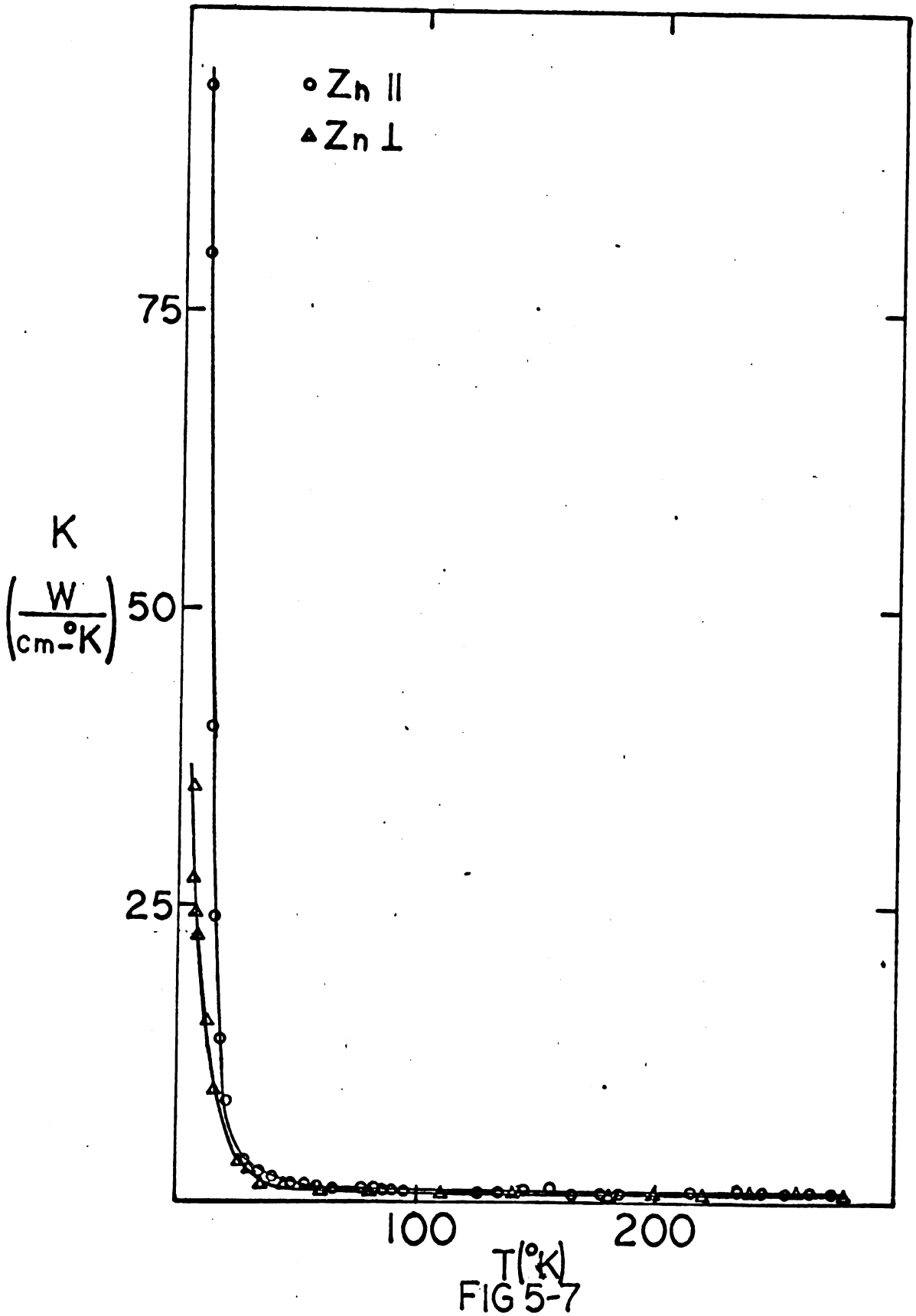

FIG 5-7

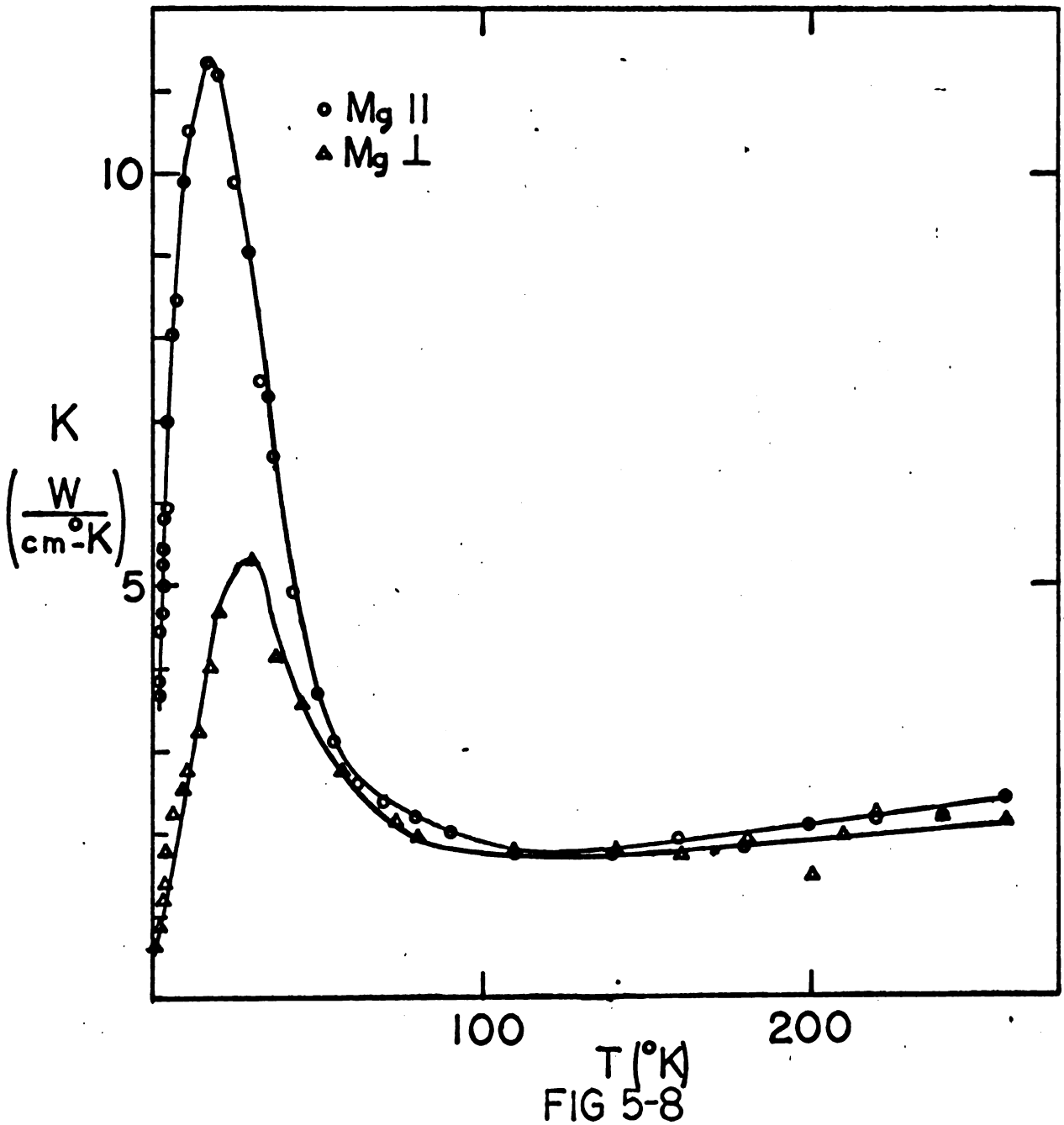

FIG 5-8

C. Accuracy

Systematic Error:

Propagation of errors from the expected accuracies quoted in the section on electronics leads to an overall estimated accuracy of 5 - 7% in the thermopower and, perhaps, 7 - 9% in the thermal conductivity. The latter is necessarily less accurate because it depends on the difficult measurement of an average area to put in the geometrical form factor in the defining equation for the thermal conductivity. In general, two approaches were taken to measuring the area, as outlined in Chapter 3. The resultant areas are internally consistent to within 2% and probably are good to 3 or 4%.

Random Error:

The method of taking slopes helped to eliminate errors due to stray thermal voltages which are relatively constant in time. But short term fluctuations will show up as scatter in the raw data straight lines. Presumably, taking a sufficient number of points on these plots will average out such fluctuations. Drifts with rise times on the order of minutes, however, are not removed by this scheme. Errors arising from this effect will appear as scatter in the final analyzed results.

We estimate the average overall error in the thermopower data to be on the order of .05 $\mu V/^{o}K$. Estimates of error in the thermal conductivity are harder to give, because of the tremendous range of values covered. Certainly near the

peaks in Cd and Zn the results are at best rough estimates of the thermal conductivity. In regions where K is not changing rapidly, probably 10% is a fair number to assign to the expected accuracy of the measurements.

D. Fermi Surfaces

In this section we describe features of the Fermi surfaces of Cd, Zn and Mg important to this investigation.

A detailed knowledge of the topology and absolute measurements of the Fermi surface is essential to the evaluation of equation 2-XIX, for example. Similarly, we require a complete set of calipers to evaluate the possibilities implied by 2-XXV.

Figure 5-9 is an O.P.W. model for the Fermi surface of magnesium[32]. Shown reduced into the 1st Brillouin zone (a) is a 2nd band hole surface usually referred to as the "monster". The piece labelled (b) is a 1st band hole pocket, hereafter referred to as a "cap". Inset (c) pictures a 3rd band electron surface usually called the "needle". Inset (d) is the 3rd band "lens". Inset (e) is the last electron sheet in the 3rd band often called the "butterfly". The last sheet, (f), is an electron surface in the 4th band referred to in this work as the "cigar".

This surface is typical of all three of the hexagonal metals we have studied. Certain details are altered in the O.P.W. picture for the other two metals. These changes are brought about by the different c/a ratios of the other metals.

Zinc's c/a ratio is approximately 1.831.[33] In this

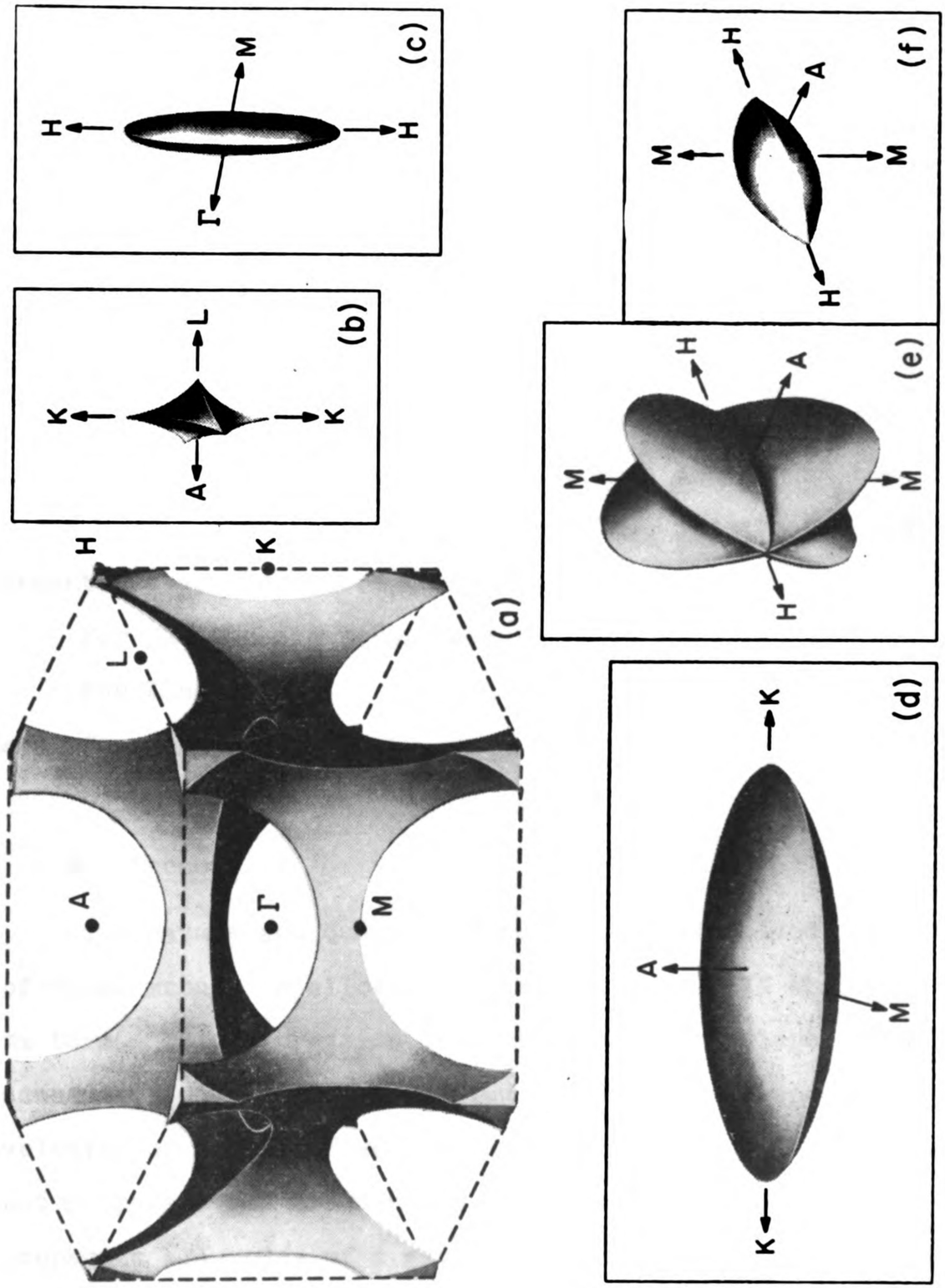

Fig. 5-9

case the O.P.W. surface changes in the following fashion. The needles shrink considerably in girth and tend to become more representative of their name. The first zone caps enlarge, and the monster arms enlarge[34].

The trends observed in Zn are carried further in Cd. The reason for this is the rather higher c/a axis ratio in Cd: 1.864. Harrison has calculated[34] that the needles will disappear at a critical axis ratio of 1.8607, which Cd has exceeded.

There is a host of experimental evidence supporting the topological truth of the above statements concerning the Fermi surfaces of these Group II metals. We cite the most recent and complete work here.

For Cadmium see references 35 through 38 ,
for Zinc " " 38 through 40 ,
and for Magnesium " " 41 through 43 .

E. Phonons

The nature and quality of the phonons involved in each of these metals is allowed for in equation 2-XIX through the $\nabla\omega$ term. This expression is a measure of the dispersion, since in a dispersionless medium $\nabla\omega$ is just the constant velocity of sound. However, our discrete metal lattices do not propagate all frequencies at the same speed, nor do they propagate all modes of a given frequency at the same speed. To make matters worse, in these hexagonal materials a given frequency and mode travel with different speeds in different directions. But this dispersion relation is one of the

results of neutron scattering experiments. Such dispersion data have been obtained for Mg and Zn. Unfortunately, the absorption cross section for thermal neutrons is very large (2500 barns) in Cadmium -- making scattering experiments impossible.

At least in the cases of Mg and Zn the question of what to insert for $\nabla\omega$ is thus solved insofar as the present dispersion data is complete.

F. An Order of Magnitude Calculation

Faced with the herculean task involved in evaluating equation 2-XIX we must necessarily demure and resort to approximation. We will see in the next section that we attribute the low temperature thermopower in Zn to the needles. At first sight it is questionable whether such a small section of Fermi surface could make a measurable contribution. We therefore make the following rough calculation to see if the argument is reasonable.

At very low temperature (in Zinc, for example) we expect the needles to make the largest contribution to the perpendicular component of the phonon drag. This is because they are the smallest part of the Fermi surface and only very small q's are required to give a complete reversal in electron velocity and hence make a large $(\underline{v}_i - \underline{v}') \cdot \underline{q}$ contribution. At such temperatures ($\sim 2.5^{\circ}K$) we expect the phonon-phonon interaction to be small and furthermore that for the phonon flux perpendicular to the needles only phonon-electron transitions of

the type shown in figure 5-10will predominate. We therefore put $\alpha = 1$.

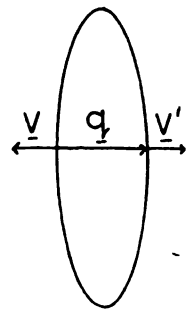

Figure 5-10

We drop the sum over $\underline{k}$ and ℓ and the sum over lattice modes as well, assuming only phonons with $\underline{q}$'s the size of these needles will contribute, ie. ~.02 $\overset{o-1}{A}$. Note that N is the number of atoms in the sample and just normalizes this last sum over lattice modes. Hence, it is set to 1 in this calculation. $\nabla\omega$ is set equal to the sound velocity, 3700 m/sec. from the Handbook of Chemistry and Physics. $\frac{dN_{oj}}{dT}$ is just:

$$\frac{dN_{oj}}{dT} = \frac{1}{T} \frac{x}{2 \sin h^2 x} , \quad x = \frac{\hbar s q}{2kT}$$

and is roughly $\frac{.12}{^oK}$ in magnitude.

The last factor is evaluated as follows:

$$(\underline{v} - \underline{v}') = -2v_f = -2\frac{\hbar r_f}{m^*}$$

Where we insert .01 $\mathring{A}^{-1}$ for r_f it is seen that m^* cancels out in this approximation.

Collecting all this together we obtain -19 $\mu V/^oK$. This is several orders of magnitude too large considering our measured value of -.1 $\mu V/^oK$.

On the other hand, it may be seen that even such small pieces of surface may contribute considerably to the phonon drag.

G. The Working Hypothesis

In Chapter 2 we argued that in some crude way we could associate with each piece of Fermi surface a characteristic temperature expressed by equation 2-XXV. At this temperature we expect appreciable numbers of large angle scattering events across the piece in question. These events hopefully will show up as influencing the observed thermopower, tending to make it more positive in the cases of transitions across hole regions and more negative in the case of transitions across electron regions, as described in figure 2-3 and the discussion surrounding it.

In this spirit we have constructed a compendium of the results of equation 2-XXV particularized to each metal through the Debye temperature and the lattice parameters.

Lattice parameters and Θ_D's are collected in Table 5-1. It might be pointed out that the Debye temperature is by no means a fixed constant. At least for Cd and Zn it is quite temperature dependent. We have allowed for this in a rough way using the data of reference (44) for Zn and Cd. The calipers of each of the various Fermi surfaces, together with their equivalent temperatures, are shown in Table 5-2. Caliper data were culled from the sources listed in section D of this chapter. Where only areas are quoted, simple assumptions were made with the O.P.W. model as a guide in converting to calipers.

Blank entries indicate a topologically impossible transition, while question marks stand for calipers that we were unable to obtain from the present data on the Fermi surfaces. "e" and "h" represent electrons and holes, respectively.

	Cd	Zn	Mg
c/a	1.864 (37)	1.831 (39)	1.623 (42)
c ($\mathring{A}$)	5.531 (37)	4.861 (39)	5.174 (42)
a ($\mathring{A}$)	2.968 (37)	2.655 (39)	3.188 (42)
Θ_D (^oK)	188 (44)	308 (44)	350 (45)

Table 5-1

Surface \ Metal		Cd		Zn		Mg	
		($\AA^{-1}$)	T(^{o}K)	($\AA^{-1}$)	T(^{o}K)	($\AA^{-1}$)	T(^{o}K)
1st band caps (h)	$\perp$	.3	22	.3	25	.045	8
	$\parallel$	?	?	?	?	.166	47
2nd band monster waist (h)	$\perp$	-	-	.074	17	.189	38
	$\parallel$	-	-	.026	6	.242	70
2nd band monster tentacles (h)	$\perp$	.31	24	.33	35	?	?
	$\parallel$	-	-	-	-	.09	27
3rd band needles (e)	$\perp$	-	-	.02	2.5	.189	34
	$\parallel$	-	-	-	-	?	?
3rd band lens (e)	$\perp$	1.43	128	1.59	150	1.17	208
	$\parallel$	.5	83	.53	100	.30	87
3rd band butterfly (e)	$\perp$	.7	62	?	?	.68	120
	$\parallel$	?	?	.73	140	.77	222
4th band cigars (e)	$\perp$	.03	3	.11	15	.16	29
	$\parallel$	.03	5	.11	22	.16	46

Table 5-2

H. Comparison with Experimental Results

In view of the difficulties associated with any exact calculation we hope to establish tentative correlation of our results with details of the Fermi surfaces using the ideas presented at the end of Chapter 2. At least such a comparison will help guide future calculations by suggesting the relative importance of the various terms in 2-XIX.

We assume that phonon drag will still be an appreciable process up to the vicinity of the Debye temperature, although this is a difficult thing to assess.

Let us look first at each metal separately and then consider similarities and differences among them.

- Cadmium

The most striking feature of the data (see figure 5-1) on Cd is the large positive peak at 20°K in the perpendicular component. A glance at Table 5-2 shows two candidates, the first band caps and the 2nd band monster tentacles, both with expected contributions near 20°K. This peak is quite sharp and suggests that a relatively strong negative contribution may be starting in. One can almost call the minimum at 130°K a "peak" although it certainly is not as well defined. We suggest that transitions involving the 3rd band Butterfly (characteristic temperature: 62°K) and the 3rd band Lens (T_c = 128°K) are involved in bringing about this negative contribution. At this point we must appeal to diffusion processes to explain the rapid rise as

room temperature is approached. In any case phonon-phonon interactions begin to limit the phonon drag by reducing α in 2-XIX.

The situation is somewhat different in the parallel component. In this case the caps are spanned the long way and present much less area to the phonon flux while transitions across the monster tentacles are unlikely in this direction. We feel that this may explain the absence of a large positive peak in this component. The small negative dip at $12^{o}K$ is quite interesting and may be the result of interactions involving the 4th band cigars ($T_c = 5^{o}K$).

At higher temperatures the lens ($T_c = 83^{o}K$) should be an effective force in holding the thermopower negative. It presents a large area to the phonons and thus should provide many opportunities for the sort of scattering events needed. This would help explain the fact that the parallel component lies below the perpendicular component.

There still remains the question of the cigars' influence on the perpendicular component. This sheet should be just as effective in both symmetry directions. It would appear to be a case of the contribution of one piece being swamped by the larger effect of another piece of surface.

- Zinc

The perpendicular component of Zinc has three features that we shall examine.

The first of these is a small negative-going dip near

2.2°K. (See figures 5-2 and 5-12). Table 5-2 shows that the needles (3rd band electron surfaces) have a characteristic temperature of 2.5°K in our scheme.

In the vicinity of 30°K we find a somewhat broad positive peak. We presume that three pieces contribute to this rise: 1) the Monster waist (T_c = 17°K), 2) the Caps (T_c = 25°K), and 3) the Monster tentacles (T_c = 35°K).

We tentatively attribute the negative-going drop from the 30°K peak to transitions across the lens (T_c = 150°K) and the butterflies (T_c unknown, probably between 60 and 100°K)

The relatively featureless temperature dependence above 100°K is consistent with the fact that there are no larger pieces of surface available. See the discussion below on the parallel component for further comment on this feature of the data.

The data taken for the parallel sample of Zinc has two distinct peaks, although we can only guess at the exact position of the lowest temperature peak. (figure 5-2 and 5-11)

The data suggest a positive peak near 5 or 6°K. We find in Table 5-2 an entry for the monster waist at a characteristic temperature of 6°K.

Near 32°K we find a large negative peak. The closest entry in Table 5-2 is for the cigars at 22°K. However, the decay of this peak does not seem capable of explanation in terms of the present hypothesis.

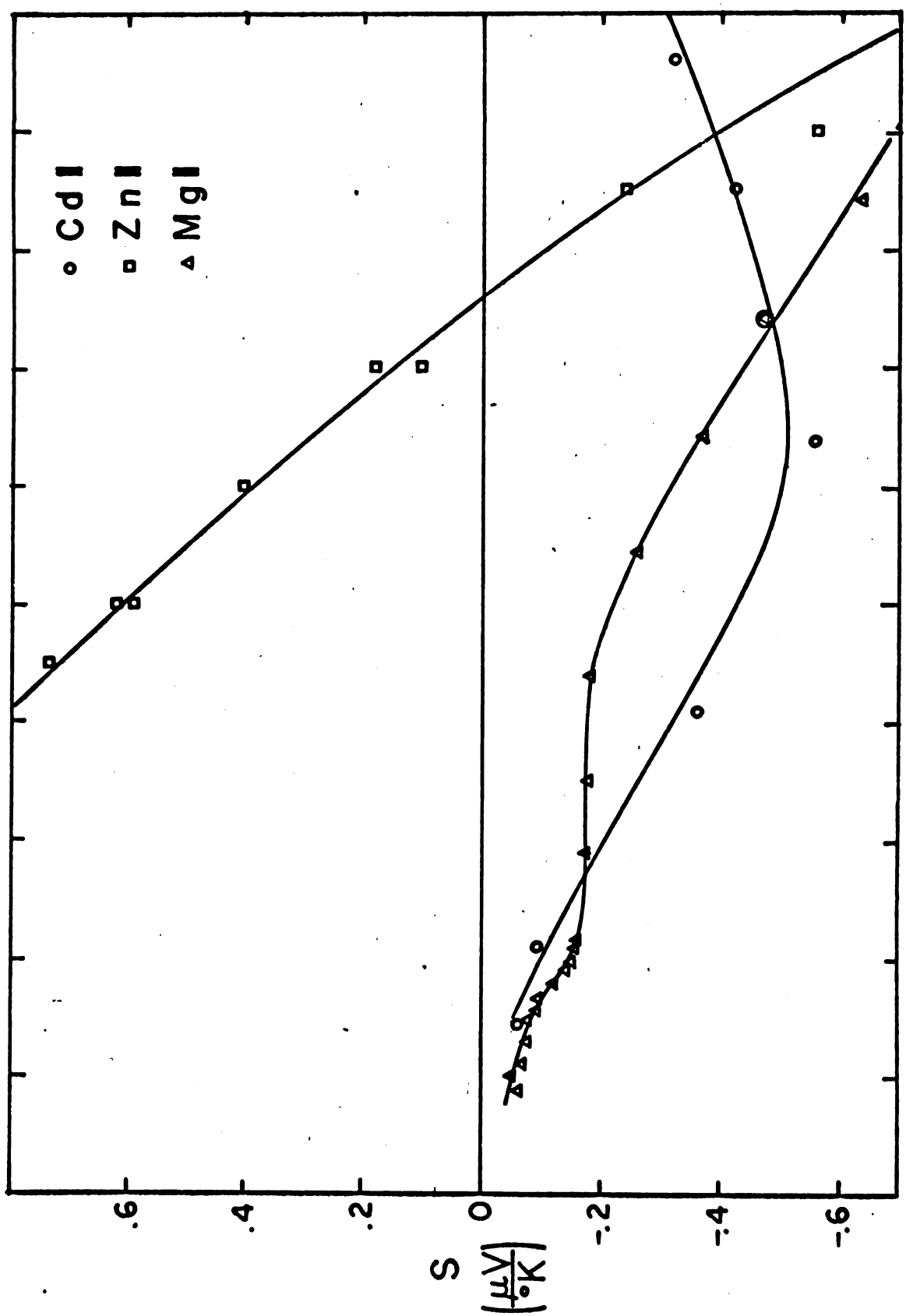

FIG 5-11

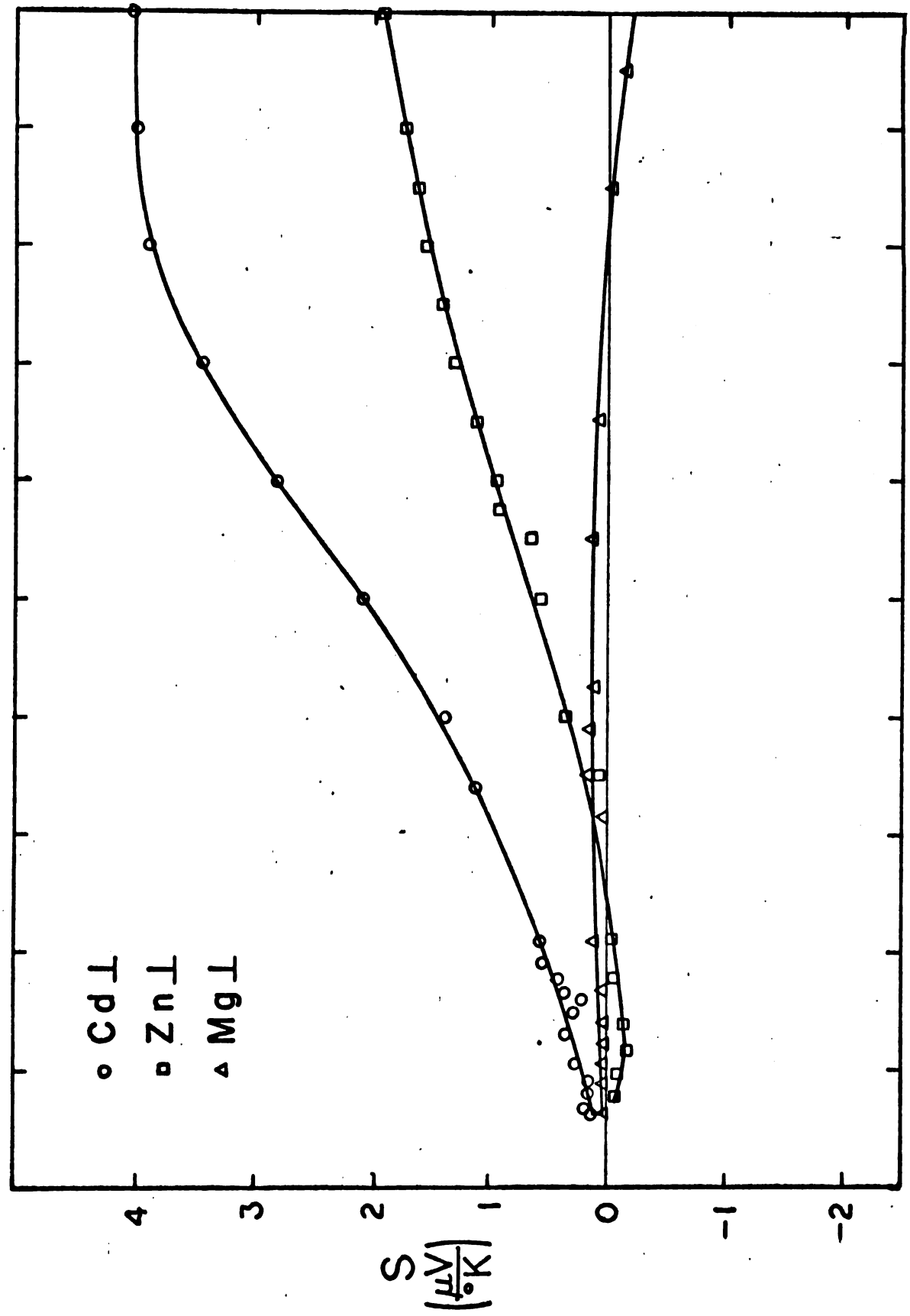

FIG 5-12

- Magnesium

Magnesium perpendicular has two distinct peaks (see figures 5-3 and 5-5), a small positive one at 8 or 9°K and one of opposite sign near 80°K.

Table 5-2 shows an entry for the 1st band Caps at a characteristic temperature of 8°K.

The 4th band Cigars are the electron surfaces with the lowest characteristic temperature (29°K). Next in line are the Butterflies at 120°K and finally the Lens at 208°K. The initial drop in thermopower centered at 30°K may be associated with the Cigars. However, the abundance of electron surfaces makes this unclear. In this instance we may be able to blame the decay of the 80°K peak on the Monster waist (T_c = 38°K) and possibly on the Monster tentacles (T_c unknown, probably around 70°K).

Magnesium parallel remains negative over the whole range of temperatures for which we have taken data. There is a small positive going tendency near 6°K. As mentioned above (Section 5), however, it is distinctly possible that this is associated with a resistance minimum anomaly. For our purposes we shall so regard it.

We attribute the absence of a more defined positive peak to the shape of the Caps. q vectors capable of spanning these sheets in the parallel direction arise at a somewhat higher temperature than those required to span them in the perpendicular direction. The positive tendency at higher

temperatures is then swamped by the preponderance of electron surfaces seen by the advancing phonons. Admittedly, this is an hypothesis tailored to fit the facts, but we have little recourse.

We attribute the steep descent centered about $22^{\circ}K$ to the Cigars ($T_c = 46^{\circ}K$) and especially the Lens ($T_c = 87^{\circ}K$).

There seems to be a positive kink at about $100^{\circ}K$, possibly associated with the Monster waist ($T_c = 70^{\circ}K$), and/or the Caps ($T_c = 47^{\circ}K$).

- Similarities and Dissimilarities

We shall organize our discussion of the comparative features of the thermopowers according to the pieces of Fermi surface to which we have ascribed the various observed tendencies. We first treat the Caps.

The Caps in Cd and Zn are of comparable size and have almost the same assigned temperatures. The Caps in Mg are considerably smaller, and are assigned a lower temperature. Consonant with this observation, we find that the positive peaks in Cd and Zn perpendicular are quite similar, while in Mg perpendicular the peak falls at a much lower temperature. Unfortunately, information on calipers of the Caps in the parallel direction is not available for Cd and Zn. For this reason we do not attempt to base any speculation on their effects.

The Monster waist has been pinched off in Cd, leaving six unconnected (in the parallel direction) pockets. We therefore do not expect a contribution from this surface in Cd.

We have associated the positive rise in Zn parallel below 15°K to the waist portions of the Fermi surface. The lack of such a rise in Cd parallel implies that such a correlation is not unwarranted. We have suggested that the positive wrinkle in Mg near 100°K may also be due these waists. This correlation is not as clear cut as the others. Correlations among the perpendicular data are not apparent.

The Monster tentacles pose a possible connection between the location of the two positive peaks in Cd and Zn perpendicular. The effect of the increased width of these pieces in Zinc may be to help shift the peak to somewhat higher temperatures in Zinc.

If our assignment of the 2.2°K negative dip in Zinc perpendicular to the 3rd band Needles is correct, then the absence of Needles in Cadmium and a similar dip in Cd is striking evidence for the present hypothesis. Similarly, the larger size of these Needles in Magnesium and the absence of a similar dip further corroborates these ideas. This depends on the anomalies in Magnesium near 6°K being due to resistance minima associated effects.

The Lens is one feature that is common to all three metals and is not too different in dimensions among them.

This sheet is a strong contender for explaining the general tendency of all the parallel data to lie more negative than the perpendicular data. The area (and thus the number of scatterable states) that the Lens presents to phonons travelling parallel to the c-axis is a good deal larger than that presented to phonons travelling in perpendicular directions. We also note that the Lens is not as thick in Magnesium and that the parallel negative peak in Magnesium occurs at a lower temperature than in Cd and Zn.

There are no pronounced effects in the experimental thermopowers which can be ascribed to the Butterflies for the three metals. Part of the problem here is the lack of data on these sheets.

We suggest that the 4th band Cigars are responsible, at least in part, for the differences in the parallel components of the thermopowers of the three metals between 0 and $50^{\circ}K$. As these pieces increase in size going from Cd to Mg, we find an increase in the size of the negative peak and, at the same time, a shifting to higher temperatures. On the other hand, these pieces should be just as effective on the perpendicular components, but we see nothing suggestive of their presence in this instance.

6. Conclusions

We have attempted to relate the observed temperature dependence of the thermopowers of Cd, Zn, and Mg to detailed features of their Fermi surfaces, using a simple model for the phonon drag mechanism. We find it possible to establish a good measure of correlation, although many questions are left unanswered.

For example, an alternative explanation of the disappearance of detail in the data above 40 degrees in Cd and Zn and above 100 degrees in Mg is possible. It is argued[47] that the rapid disappearance of the peak in the lattice conductivity of Copper is in part due to the onset of phonon-phonon U-process. This occurs near $\Theta_D/10$ for dilute Copper alloys. If such is the case in these metals it could well explain the lack of detail in the data at high temperature and the dying out of the peak. This would occur through the rapid diminution of α in 2-XIX due to the onset of phonon processes not involving electrons.

Still, there is evidence* that phonon drag may persist in appreciable amounts up to room temperature in Aluminum.

We suggest a possible method of removing this impass. If one were to make dilute single crystal alloys of these metals among themselves, then perhaps the question of which details could be associated with phonon drag could be answered. This is possible for the following reasons.

---

* J. Bass, private communication, in press, Phys. Rev.

Dilute alloying should not significantly change the Fermi surfaces because the metals are isoelectronic. (Care must be taken here so as not to drastically alter the c/a axis ratios.) The ionic masses of Mg and Cd, say, are quite different, and thus the effect is to introduce very effective phonon scatterers into the lattice. Hence, one should see a quenching out of the phonon-drag effects, while the diffusion effects should remain essentially unaltered.

References

1. J. P. Jan and W. B. Pearson, Phil. Mag. 8, 911 (1963)
2. P. G. Klemons, C. VanBaarle and F. W. Gorter, Physica 30, 1470 (1964)
3. J. S. Dugdale and M. Bailyn, Phys. Rev. 157, 485 (1967)
4. J. M. Ziman, Adv. Phys. 10, 1 (1961)
5. E. Gruneisen and E. Goens, Z. Phys. 37, 278 (1926)
6. Physical Properties of Crystals, J. F. Nye, Oxford at the Clarendon Press (1957), p. 225
7. ibid, p. 227
8. ibid
9. M. Kohler, Ann. Phys. 40, 196 (1941)
10. ibid
11. F. J. Blatt, R. H. Kropschot, Phys. Rev. 118, 480 (1960)
12. The Theory of the Properties of Metals and Alloys, N. F. Mott and H. Jones, Clarendon Press, Oxford, England, (1936), P. 310
13. Electronic Conduction in Solids, A. C. Smith, J. F. Janak, R. B. Adler, McGraw-Hill (1967), p. 175
14. L. Colquitt: private communcation
15. L. J. Gurevich, J. Phys. USSR 9, 477 (1945) & 10, 67 (1946)
16. D.K.C. McDonald, Physica 20, 996 (1954)
17. Electrons and Phonons, J. M. Ziman, Oxford at the Clarendon Press (1962), p. 409
18. ibid, p. 407
19. J. M. Ziman, Adv. Phys. 10, 1 (1961)
20. M. Bailyn, Phys. Rev. 112, 1587 (1958)
21. M. Bailyn, Phys. Rev. 120, 381 (1960)

22. M. Bailyn, Phys. Rev. 157, 480 (1967)

23. J. M. Ziman, E. & P., Op.cit., P. 53

24. ibid, p. 391

25. K. S. Balain and C. J. Bergeran, Rev. Sci. Instr. 30, 1058 (1959)

26. W. R. Roach, J. C. Wheatley, A. C. Mota de Victoria, Rev. Sci. Instr. 35, 634 (1964)

27. J. W. Christian, J. P. Jan, W. B. Pearson, I. M. Templeton, Proc. Roy. Soc. (London) A245, 213 (1958)

28. E. Grüneisen and E. Goens, Z. Phys. 29, 141 (1924)

29. E. Goens and E. Schmid, Z. Phys. 37, 385 (1936)

30. unpublished

31. H. M. Rosenberg, Phil. Mag. 45, 73 (1954)

32. J. B. Ketterson and R. W. Stark, Phys. Rev. 156, 156 (1967)

33. D. F. Gibbons and L. M. Falicov, Phil. Mag. 8, 177 (1963)

34. W. A. Harrison, Phys. Rev. 118, 1190 (1960)

35. D. C. Tsui and R. W. Stark, Phys. Rev. Lett. 16, 19 (1965)

36. A.D.C. Grassie, Phil. Mag. 9, 847 (1964)

37. M. R. Daniel and L. Mackinnon, Phil. Mag. 8, 537 (1963)

38. D. F. Gibbons and L. M. Falicov, Phil. Mag. 8, 177 (1963)

39. A. S. Josheph and W. L. Gordon, Phys. Rev. 126, 489 (1962)

40. W. A. Harrison, Phys. Rev. 126, 497 (1962)

41. M. G. Priestly, Proc. Roy. Soc. (London) A276, 258 (1963)

42. J. B. Ketterson and R. W. Stark, Phys. Rev. 156, 156 (1967)

43. L. M. Falikov, Phil. Trans. Roy Soc. Ln. A255, 55 (1963)

44. P. L. Smith and N. M. Wolcott, Phil. Mag. 8, 854 (1956)

45. Solid State Physics, vol. 16, C. A. Gschneidner, Jr.

46. Metals Handbook, The American Society for Metals, Cleveland, Ohio (1948), p. 986

47. M. Garber, B. W. Scott, F. J. Blatt, Phys. Rev. 130, 2188 (1963)

Appendix 4-1

Magnesium Solder

Since it is not possible to solder directly to Magnesium with Indium, the Mg samples were first tinned with a special solder[46]. Its composition is as follows:

60% Cd

30% Zn

10% Sn

This alloy melts at about 157°C. No flux is used, but the Mg must be brightened and brought near 150°C, where tinning will start to occur. Both the cold end of the Mg samples and a small region near the ΔT thermocouple probes were tinned with this alloy. The cold end was then tinned with In over the alloy solder layer, using Zn Cl_2 non-corrosive paste flux, while the probe areas were tinned with Wood's metal using Sta-Clean as flux.

This procedure made it possible to use the same methods of sample and probe attachment as employed in the other materials.

Appendix 4-2

Heaters

The apparatus employed three separate heaters. Two of these were wound around the inner vacuum can on a layer of cigarette paper and cemented down with G.E. 7031 varnish. The power heater was wound of 12 ohm per foot Karma alloy wire* and was about 100 ohms resistance. The control heater was made of 33 ohm per foot Manganin wire with a total resistance of ~ 50 ohms.

The remaining heater (referred to as the ΔT heater) was wound of 33 ohm per foot Manganin. The total resistance of this heater was 47.73 ohms for all but the Mg samples. Mg parallel's heater measured 48.37 ohms while Mg perpendicular's heater was 56.14 ohms.

Table 4-2-1 gives the measured temperature variation of the resistance of the Manganin wire used as a ratio of its value at a given temperature to that at room temperature. These numbers were used in correcting for the power input in the calculations of the thermal conductivities.

*Source: Driver-Harris Company, Harrison, New Jersey

Table 4-2-1

R(T) for Manganin

T(^{o}K)	R(T)/R(294)
4.3	.8862
6.1	.8865
10.1	.8906
20.1	.8958
30.0	.9036
40.1	.9112
60.0	.9261
80.0	.9398
103.6	.9540
140.2	.9689
178.1	.9809
216.4	.9952
255.7	.9999
294.1	1.0000

Appendix 4-3

Thermocouples

Both the average temperature of the sample and the gradient between voltage probes were measured with special Gold - .02 atomic percent Iron vrs. Chromel thermocouples.*

The thermocouples were calibrated from 1.5 to 310 by measuring their output as a function of temperature relative to helium and nitrogen baths. This data was smoothed, interpolated to equispaced intervals, differentiated, and smoothed again using a program developed to analyze thermopower data from wires. The input data and final results are shown below in the actual computer output. The helium range was covered using a calibrated Ge resistance thermometer; in the nitrogen range a platinum thermometer was employed.

The accuracy of this calibration is estimated to be better than 1% or 0.3 K^{o}, which ever is smaller.

The first table shows, reading columns from left to right, the Ge resistance read, the absolute temperature and the thermocouple output. The last column is redundant in this case; normally, it would have been the result of adding the thermal emf. of pure lead to column 3.

The second table below gives in the first column the equispaced temperatures and in column 2 the corresponding

---

*Source: Sigmund Cohn Corp., Mount Vernon, New York

parabolically interpolated emf.'s. The third column is the smoothed version of column 2, and the last column is the derivative of the emf. vrs. temperature table with respect to temperature. This is referred to as dV/dT in the text and is the voltage sensitivity of the thermocouple relative to small changes in temperature.

The last two tables are similar except now the Platinum thermometer has been used to measure temperature.

HE CALIB, AU-FE TC 4.18.67

TOTAL NUMBER OF INPUT POINTS= 33

TOTAL NUMBER OF OUTPUT POINTS= 43

DELTA T= 2 DEGREES KELVIN

GE RES (OHMS)	TEMP (DEG KELVIN)	EMF1 (MICROVOLTS)	EMF2 (MICROVOLTS)
1048.100000	4.234747	0.800000	0.800000
1045.950000	4.238831	1.000000	1.000000
918.260000	4.501643	4.300000	4.300000
721.610000	5.018496	11.200000	11.200000
584.420000	5.516253	16.400000	16.400000
479.830000	6.011688	22.400000	22.400000
329.440000	7.035095	34.900000	34.900000
239.670000	8.018260	47.600000	47.600000
178.830000	9.033178	61.200000	61.200000
139.290000	10.031620	74.700000	74.700000
93.363000	12.017047	102.000000	102.000000
68.495000	14.020004	128.600000	128.600000
53.638000	16.042481	155.700000	155.700000
44.179000	18.010143	181.700000	181.700000
37.129000	20.107322	207.700000	207.700000
36.195000	20.434885	213.000000	213.000000
28.304000	24.110525	258.700000	258.700000
22.241000	28.502804	311.600000	311.600000
18.912000	31.985372	352.000000	352.000000
18.541000	32.438606	357.600000	357.600000
16.081000	35.949407	397.900000	397.900000
13.356000	41.165358	458.400000	458.400000
11.958000	44.805205	500.600000	500.600000
10.460000	49.722006	558.900000	558.900000
9.251000	54.900151	620.500000	620.500000
8.362000	59.786500	678.700000	678.700000
7.489000	65.897645	756.100000	756.100000
7.060000	69.618644	803.500000	803.500000
6.546000	74.964776	873.800000	873.800000
6.151000	80.013691	940.300000	940.300000
5.816000	85.114786	1012.700000	1012.700000
5.781000	85.697330	1021.800000	1021.800000
5.536000	90.170099	1088.100000	1088.100000

HE CALIB, AU-FE TC 4.18.67

T (DEG KELVIN)	E3 (MICROVOLTS)	E4 (MICROVOLTS)	S (UV/DEG KELVIN)
5,000000	10,979449	10,398976	12,139034
7,000000	34,459191	35,318591	12,764417
9,000000	60,753460	61,191938	13,159473
11,000000	88,131426	87,711364	13,360117
13,000000	115,024318	114,569219	13,402263
15,000000	141,778931	141,454345	13,334861
17,000000	168,546500	167,878018	13,164232
19,000000	192,262021	193,860124	12,948225
21,000000	220,111021	219,526624	12,706163
23,000000	245,030079	244,736849	12,444225
25,000000	269,588074	269,347239	12,195978
27,000000	293,744842	293,701981	11,959485
29,000000	317,083049	317,142508	11,771346
31,000000	340,097019	340,536689	11,655008
33,000000	364,021367	363,763874	11,581387
35,000000	386,968403	386,949798	11,561659
37,000000	410,088404	410,148246	11,568701
39,000000	433,287766	433,290360	11,574483
41,000000	456,482486	456,372987	11,609257
43,000000	479,568692	479,656649	11,667117
45,000000	502,906209	503,056842	11,738984
47,000000	526,601360	526,598912	11,798271
49,000000	550,327299	550,309996	11,823883
51,000000	574,095988	574,057175	11,835143
53,000000	597,886490	597,715899	11,864067
55,000000	621,656479	621,389301	11,924359
57,000000	645,109230	645,281069	12,036581
59,000000	669,110942	669,520422	12,202948
61,000000	694,025238	694,144230	12,394509
63,000000	719,330951	719,120072	12,573637
65,000000	744,696169	744,462170	12,720638
67,000000	770,011456	770,037013	12,839683
69,000000	795,532358	795,823747	12,922594
71,000000	821,653103	821,705625	12,958319
73,000000	847,950081	847,736509	12,987855
75,000000	874,246155	873,847111	13,063179
77,000000	899,988719	899,967136	13,210833
79,000000	926,536706	926,436375	13,445952
81,000000	953,278952	953,695245	13,773695
83,000000	981,097910	981,713136	14,201042
85,000000	1010,927017	1010,576307	14,675928
87,000000	1041,109519	1040,375590	15,173369
89,000000	1070,755583	1071,201818	15,668380

THIRD DIFFERENCES

-3,0765-001	-3,0765-001	-3,1116-001	-4,8872-001	1,9887-002
1,2596-001	-1,4067-001	-1,4356-001	3,4419-001	-6,5857-001
8,6787-001	-1,2065-001	1,2573-001	5,3785-002	-6,8858-002
-3,1525-003	2,6052-001	-8,4503-002	2,5345-002	2,7137-002
-1,3292-001	-1,2455-001	1,0313-001	2,0369-001	1,2922-001
3,6871-002	-3,2421-002	1,4222-002	-1,3351-001	-2,0853-002
-1,1675-001	5,3862-002	-6,9288-002	-7,0294-002	3,3979-001

LN2 CALIB, AU-FE TC NO, 2

TOTAL NUMBER OF INPUT POINTS= 39

TOTAL NUMBER OF OUTPUT POINTS= 47

DELTA T= 5 DEGREES KELVIN

PT RES (MICROVOLTS)	TEMP (DEG KELVIN)	EMF1 (MICROVOLTS)	EMF2 (MICROVOLTS)
9779,400000	78,205914	18,800000	18,800000
9911,400000	78,795162	29,200000	29,200000
9961,200000	79,017529	33,100000	33,100000
10012,800000	79,247968	36,400000	36,400000
10626,300000	81,990504	77,000000	77,000000
11049,400000	83,884843	104,000000	104,000000
11481,100000	85,820197	130,000000	130,000000
11948,900000	87,920277	159,900000	159,900000
12419,100000	90,034182	189,400000	189,400000
13307,200000	94,035280	246,400000	246,400000
14199,900000	98,068296	304,200000	304,200000
15075,600000	102,035498	362,200000	362,200000
15954,100000	106,026375	421,400000	421,400000
16845,300000	110,086215	482,800000	482,800000
17703,800000	114,007819	543,000000	543,000000
18575,400000	118,000003	605,500000	605,500000
22937,200000	138,138210	934,900000	934,900000
23973,500000	142,960892	1015,800000	1015,800000
25050,900000	147,989796	1101,000000	1101,000000
26148,000000	153,125960	1190,000000	1190,000000
27184,800000	157,993663	1274,400000	1274,400000
28268,800000	163,096956	1363,500000	1363,500000
29368,300000	168,287401	1455,200000	1455,200000
31440,800000	178,108349	1631,900000	1631,900000
32466,600000	182,986523	1720,600000	1720,600000
33526,900000	188,040206	1813,600000	1813,600000
34573,200000	193,038164	1905,900000	1905,900000
36043,000000	200,076807	2036,400000	2036,400000
38078,200000	209,855465	2220,600000	2220,600000
40177,700000	219,980074	2413,800000	2413,800000
42310,400000	230,300821	2612,600000	2612,600000
46394,600000	250,160256	3002,800000	3002,800000
48324,800000	259,587720	3190,300000	3190,300000
50612,900000	270,798288	3416,600000	3416,600000
52543,200000	280,286625	3609,800000	3609,800000
54509,200000	289,981545	3806,300000	3806,300000
56494,300000	299,805566	4006,900000	4006,900000
58458,000000	309,562315	4206,800000	4206,800000
59493,500000	314,724456	4315,900000	4315,900000

LN2 CALIB, AU-FE TC NO, 2

T (DEG KELVIN)	E3 (MICROVOLTS)	E4 (MICROVOLTS)	S (UV/DEG KELVIN)
79,000000	32,818083	33,393093	14,244761
84,000000	105,505321	104,312970	14,131467
89,000000	174,914656	175,126260	14,155172
94,000000	245,895907	246,262110	14,293292
99,000000	317,745358	318,149671	14,523240
104,000000	391,197738	391,204881	14,824695
109,000000	466,280451	466,339788	15,175343
114,000000	542,878791	543,221564	15,536503
119,000000	621,536476	621,867040	15,871979
124,000000	702,221426	702,039961	16,152745
129,000000	783,743545	783,455879	16,386229
134,000000	866,102833	865,888800	16,590049
139,000000	949,298522	949,271944	16,771797
144,000000	1033,247180	1033,530428	16,948664
149,000000	1118,500479	1118,703531	17,125323
154,000000	1205,112589	1204,746969	17,298375
159,000000	1291,886739	1291,703035	17,471959
164,000000	1379,370303	1379,531261	17,649148
169,000000	1467,936898	1468,141276	17,825168
174,000000	1557,677190	1557,626074	17,993028
179,000000	1648,034409	1648,080528	18,148897
184,000000	1739,223910	1739,271887	18,294606
189,000000	1831,301546	1831,080696	18,427843
194,000000	1923,629894	1923,463978	18,549089
199,000000	2016,322296	2016,491772	18,669503
204,000000	2110,017856	2110,156524	18,794142
209,000000	2204,391581	2204,435685	18,918685
214,000000	2299,468769	2299,342658	19,040482
219,000000	2395,019122	2394,863426	19,160039
224,000000	2490,908613	2490,938500	19,277959
229,000000	2587,393322	2587,597244	19,392499
234,000000	2684,790686	2684,844664	19,500807
239,000000	2782,724665	2782,644105	19,602356
244,000000	2881,069420	2880,933466	19,702866
249,000000	2979,824950	2979,701542	19,808955
254,000000	3078,858126	3078,923223	19,922563
259,000000	3178,536101	3178,748206	20,037156
264,000000	3279,113290	3279,263002	20,145834
269,000000	3380,155675	3380,311026	20,236287
274,000000	3481,890847	3481,696922	20,292791
279,000000	3583,653374	3583,248266	20,316868
284,000000	3684,892153	3684,948052	20,325000
289,000000	3786,339552	3786,521977	20,335041
294,000000	3888,271924	3888,170476	20,354999
299,000000	3990,425253	3990,050053	20,396793
304,000000	4091,826518	4092,264699	20,471417
309,000000	4195,055118	4194,918404	20,589865

THIRD DIFFERENCES

4,2915-001	4,2915-001	4,1594-001	9,1205-001	-3,3283-001
1,6832-002	-2,3626-001	-2,8445-001	-2,2599-001	-6,6779-002
-7,4885-002	3,9280-002	-4,4284-002	4,2293-002	-4,0470-002

Appendix 4-4

Heater Controls

Figure 4-4-1 shows the heater control circuit employed, while Table 4-4-1 lists the circuit parameters. Identical circuits were used to control both ΔT and T.

Basically, the control circuit compares the sensing voltage supplied at J5 with the reference voltage generated across R13 by B1. The difference between these two voltages is amplified by the operational amplifier, OA2, and sent through two cascaded emitter followers, Q1 and Q2 which boost the current up to levels needed to drive the heater. The gain of the operational amplifier is adjusted by varying R1 and R2 until maximum sensitivity consistent with loop stability is attained.

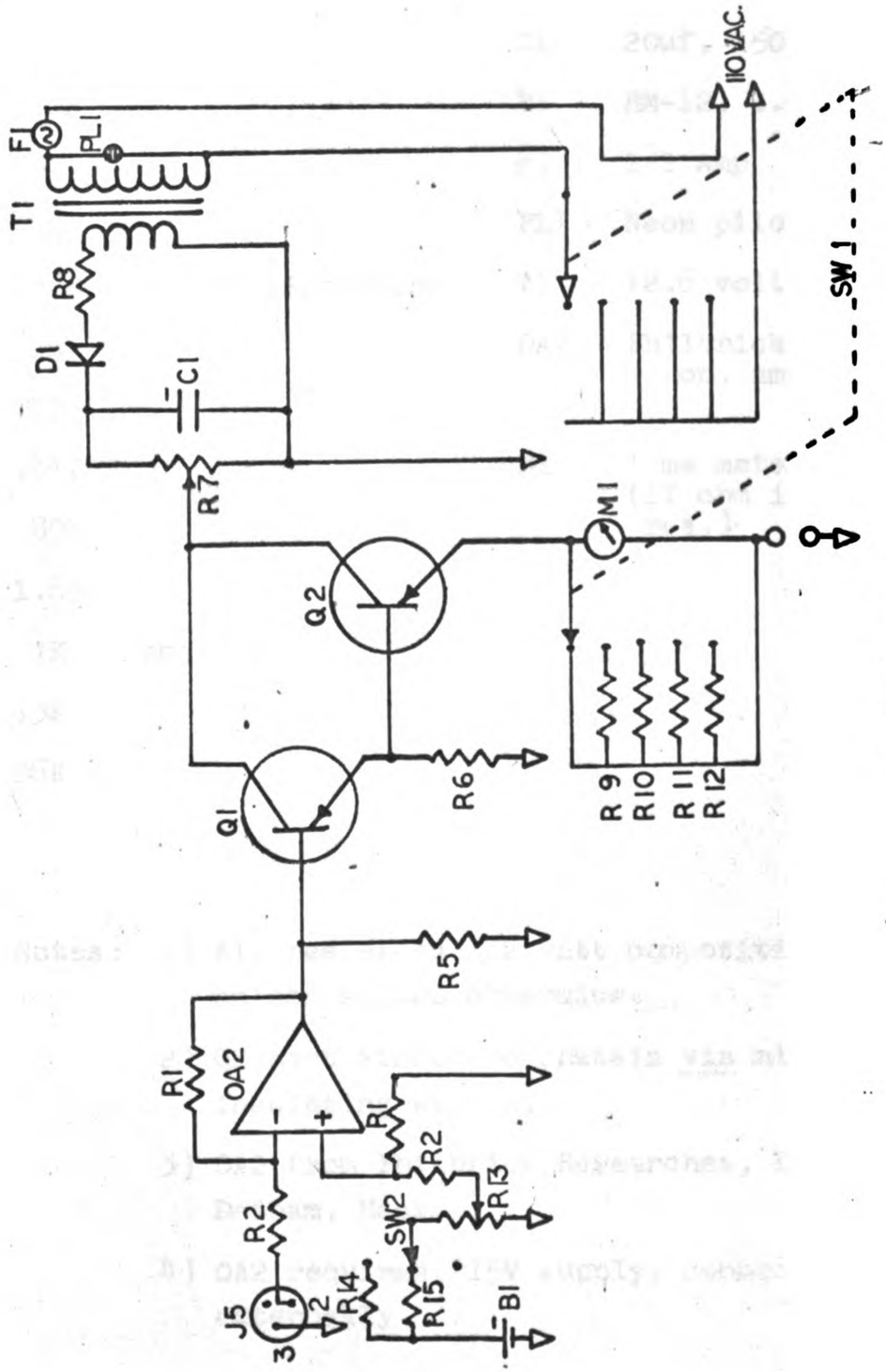
F1
PL1
T1
R8
D1
C1
R7
110VAC.
SW1
M1
Q2
Q1
R6
R9
R10
R11
R12
R5
R1
OA2
R1
R2
R13
SW2
R2
J5
3
2
R14
R15
B1

FIG 4-4-1

Table 4-4-1

R1	1M		Q1	2N107
R2	10K		Q2	2N251
R3	1M		C1	20μf, 150 WVDC
R4	22K		B1	RM-12, 1.4 VDC
R5	5M		F1	1/2 Amp
R6	2K		PL1	Neon pilot lamp
R7	200	5 watt wire wound	T1	12.6 volt, 2 Amp
R8	6		OA2	Philbrick P65 AU op. amp.
R9	.172			
R10	.347		M1	1 ma meter (17 ohm internal res.)
R11	.896			
R12	1.89			
R13	1K	helipot		
R14	13K			
R15	26K			

Notes:
1) All resistors 1/2 watt composition unless stated otherwise.
2) Q2 heat sinked to chassis via mica insulating washer.
3) OA2 from Philbrick Researches, Inc., Dedham, Mass.
4) OA2 requires ±15V supply, connected externally.

POWER SUPPLY

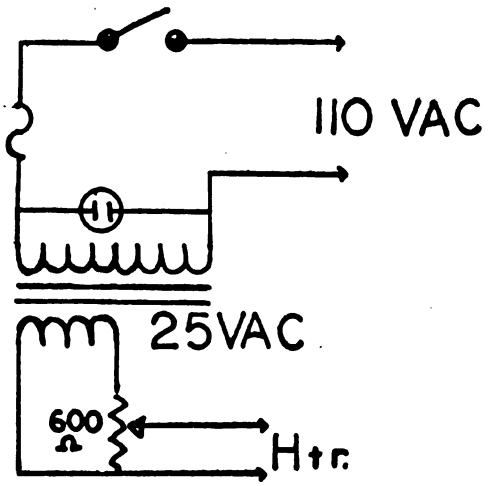

FIG. 4-4-2